A novel formulation of point vortex dynamics on the sphere: geometrical and numerical aspects

Joris Vankerschaver, Melvin Leok

20 November 2012

Abstract

In this paper, we present a novel Lagrangian formulation of the equations of motion for point vortices on the unit 2-sphere. We show first that no linear Lagrangian formulation exists directly on the 2-sphere but that a Lagrangian may be constructed by pulling back the dynamics to the 3-sphere by means of the Hopf fibration. We then use the isomorphism of the 3-sphere with the Lie group $SU(2)$ to derive a variational Lie group integrator for point vortices which is symplectic, second-order, and preserves the unit-length constraint. At the end of the paper, we compare our integrator with classical fourth-order Runge–Kutta, the second-order midpoint method, and a standard Lie group Munthe-Kaas method.

1 Introduction

Point vortices are point-like singularities in the vorticity field of an ideal fluid. First described by von Helmholtz [1858], they form a finite-dimensional singular solution of the Euler equations and are now a classical subject in hydrodynamics, see among others Lamb [1945]; Milne-Thomson [1968]; Saffman [1992]; Newton [2001].

The interest in point vortices is two-fold. On the one hand, paraphrasing Aref [2007], the description of point vortices forms a veritable playground for classical mathematics and gives rise to interesting phenomena from dynamical systems, such as periodic motions (Soulière and Tokieda [2002]; Borisov, Mamaev, and Kilin [2004]), (relative) equilibria (Kidambi and Newton [1998]; Aref [2011]), and chaotic advection and topological chaos in fluids (Boyland, Stremler, and Aref [2003]). On the numerical front, on the other hand, desingularizations of the point vortex equations, such as the classical vortex blob method of Chorin [1973] form the basis for important classes of particle methods for the Euler and Navier-Stokes equations. The idea is that the vorticity field of an arbitrary fluid can be approximated by a number of vortex blobs whose motion is then followed in time. Strong analytical estimates exist that link the behavior of the vortex blobs with the solution of the Euler equations that they approximate (Majda and Bertozzi [2002]).

On the sphere, the dynamics of point vortices was first described by Bogomolov [1977] after a model by Gromeka (see Newton [2001] for an historical overview) and is in some sense a generalization of the planar case (see also Kimura and Okamoto [1987] and Polvani and Dritschel [1993]). The relevance of point vortices of the sphere lies in the fact that they provide a first approximation of the behavior of certain geophysical flows for which the curvature of the earth is important, and which persist over long periods of time. The mathematical description of point vortices on the sphere is an area of active research: fixed and relative equilibria of the three-vortex problem were described in Kidambi and Newton [1998] (see also Pekarsky and Marsden [1998]), while more general equilibria were described in Lim, Montaldi, and Roberts [2001]; Chamoun, Kanso, and Newton [2009]; Newton and Sakajo [2011]. Conditions for the collapse of point vortex configurations on the sphere were established in Kidambi and Newton [1998] and Sakajo [2008].

Most of the research on point vortices on the sphere has focused on the existence of analytical solutions such as relative equilibria for few point vortices, but comparatively little is known about the behavior of arbitrary configurations of vortices. One of the contributions of this paper is to construct a geometric numerical integrator which is second-order accurate, preserves the geometry of the sphere, and is symplectic. As symplectic integrators are known to capture the long-term behavior of a Hamiltonian system better than classical integrators (see Marsden and West [2001]; Hairer, Lubich, and Wanner [2002]), we expect our geometric integrator to give insight into the behavior of non-equilibrium vortex configurations, even over long integration times.

1.1 Aims and contributions of this paper

The contributions of this paper are two-fold. In the first part of this paper, we construct a Lagrangian description for point vortices on the sphere in terms of pairs of complex numbers. We first review the Lagrangian description for point vortices in the plane (see e.g. Chapman [1978]; Newton [2001]; Rowley and Marsden [2002]) and then show via a simple topological argument that no (linear) Lagrangian exists for the dynamics of point vortices on the two-dimensional sphere $\mathbb{S}^2$.

We then use the *Hopf fibration*, a distinguished submersion from the three-sphere $\mathbb{S}^3$ to the two-sphere $\mathbb{S}^2$, to pull back the Hamiltonian description to $\mathbb{S}^3$, where the topological obstruction for the existence of a linear Lagrangian vanishes. We explicitly construct this Lagrangian and we show that the equations of motion give rise to a (finite-dimensional) *non-linear Schrödinger equation* on $\mathbb{S}^3$ with gauge freedom. These equations bear a remarkable similarity to the equations of motion for point vortices in the complex plane, only now the location of each point vortex is specified by a pair of complex numbers (or equivalently, a (unit) quaternion) instead of a single one.

In the second part of the paper, we design a variational numerical integrator for point vortices on the sphere using the linear Lagrangian on $\mathbb{S}^3$. We use the identification between the 3-sphere $\mathbb{S}^3$ and the Lie group $SU(2)$ of special unitary 2-by-2 matrices

to write the update equation for the integrator as a fixed-point equation in the Lie algebra $\mathfrak{su}(2)$, and we show how the discrete equations of motion are symplectic, self-adjoint, second-order, and preserve the unit-length constraint in $\mathbb{S}^3$. At the end of the paper, we compare our integrator to the classical 4th order Runge–Kutta method, as well as to a number of geometric integration methods. We show that the geometric integrators, and in particular the Hopf variational integrator, outperform Runge–Kutta in the medium run, even though they are only second-order accurate.

1.2 Background and historical overview

Linear Lagrangian formulation for planar vortices. We review here the Lagrangian and Hamiltonian descriptions of point vortices in the plane. The Hamiltonian description of point vortices on the sphere will be reviewed in Section 3.

For point vortices in the plane, the equations of motion are given in complex form by

$$\dot{z}_\alpha = -2\mathrm{i}\frac{\partial H}{\partial z_\alpha^*}. \tag{1.1}$$

Here, the z_α ($\alpha = 1, \ldots, N$) represent the locations in the complex plane of each of the vortices, and Γ_α is a real parameter which specifies the circulation around each vortex. The Hamiltonian function is given by

$$H(z_1, \ldots, z_N) = -\frac{1}{4\pi}\sum_{\alpha<\beta}\Gamma_\alpha\Gamma_\beta \log|z_\alpha - z_\beta|^2. \tag{1.2}$$

These equations can be derived from a Lagrangian which is *linear* in the velocities (see Chapman [1978]) and is given by

$$L = \frac{1}{2\mathrm{i}}\sum_{\alpha=1}^{N}\Gamma_\alpha(z_\alpha^*\dot{z}_\alpha - z_\alpha\dot{z}_\alpha^*) - H(z_1, \ldots, z_N). \tag{1.3}$$

For future reference, we point out that the linear part of the Lagrangian can be written as $\sum\Gamma_\alpha\theta(z_\alpha, \dot{z}_\alpha)$, where θ is the one-form given by

$$\theta = \frac{1}{2}\operatorname{Im}(z^*dz). \tag{1.4}$$

The exterior derivative of θ is nothing but the area form on the complex plane:

$$\mathbf{d}\theta = \frac{1}{2}\operatorname{Im}(dz^* \wedge dz) = dx \wedge dy. \tag{1.5}$$

It can be shown that the flow of the point vortex equations (1.1) preserves a weighted sum of such area forms, given by

$$\sum_{\alpha=1}^{N}\Gamma_\alpha\mathbf{d}\theta_\alpha = \sum_{\alpha=1}\Gamma_\alpha dx_\alpha \wedge dy_\alpha,$$

where $\mathbf{d}\theta_\alpha$ refers to the area form (1.5) expressed in the coordinates of the αth vortex. This is an example of a symplectic form on the phase space $\mathbb{C}^N$.

The advantage of having a Lagrangian description for the dynamics of point vortices is that the standard results for the construction of Lagrangian variational integrators (see Marsden and West [2001] for an overview) can now be applied. This is the key observation of Rowley and Marsden [2002], who constructed a class of second-order variational integrators by discretizing the Lagrangian (1.3) using centered finite differences.

Before turning to the case of point vortices on the sphere, we point out that many non-canonical Hamiltonian systems can be rephrased as Euler–Lagrange equations that come from a Lagrangian which is linear in the velocities. This observation was made by Birkhoff [1966] in his study of Pfaffian systems and was used in Faddeev and Jackiw [1988] as a starting point for the description of Hamiltonian systems with constraints. Linear Lagrangians also appear in the description of the non-linear Schrödinger equation and the KdV equation.

The dynamics of point vortices on the sphere. The equations of motion for N point vortices with strengths Γ_i, $i = 1, \dots, N$ on the unit sphere $\mathbb{S}^2$ can be written as follows (see Newton [2001]). If we denote the position vector of the ith vortex by $\mathbf{x}_i$ (so that $\|\mathbf{x}_i\| = 1$), the point vortex equations can be written in Euclidian form as

$$\dot{\mathbf{x}}_k = \frac{1}{4\pi} \sum_{j \neq k} \Gamma_j \frac{\mathbf{x}_j \times \mathbf{x}_k}{1 + \sigma^2 - \mathbf{x}_k \cdot \mathbf{x}_j}, \tag{1.6}$$

where σ is a small regularization parameter which is added to ensure that the limit of the right-hand side exists when $\mathbf{x}_k$ tends to $\mathbf{x}_j$. Note that the equations (1.6) conserve the *vortex moment*, defined as

$$\mathbf{M} = \sum_{i=1}^{N} \Gamma_i \mathbf{x}_i.$$

Non-existence of a linear Lagrangian for vortices on the sphere. In Section 3, we will review the Hamiltonian formulation for the point vortex equations (1.6). We now discuss the Lagrangian formulation, and in particular we argue that *no linear Lagrangian exists for the dynamics of point vortices on* $\mathbb{S}^2$.

For point vortices on the sphere, the phase space is the product $(\mathbb{S}^2)^N$ of N copies of the unit sphere $\mathbb{S}^2$, equipped with a symplectic form which is a weighted sum of the area forms on the individual spheres. This particular symplectic form is not exact, due to $\mathbb{S}^2$ being compact; the standard way to see this is that if it were, then $\Omega = \mathbf{d}\Theta$ for a one-form Θ on the sphere, and therefore Stokes' theorem would give

$$4\pi = \int_{\mathbb{S}^2} \Omega = \int_{\mathbb{S}^2} \mathbf{d}\Theta = \int_{\partial \mathbb{S}^2} \Theta = 0,$$

a contradiction.

This rules out the existence of a linear Lagrangian on $\mathbb{S}^2$, as such a Lagrangian would necessarily have to be of the form $L = \Theta - H$, with Θ so that $\mathbf{d}\Theta$ is the symplectic form. However, we will see that the symplectic form Ω on $\mathbb{S}^2$ can be pulled back to the three-sphere $\mathbb{S}^3$ so that the resulting form is exact. This will allow us to construct a linear Lagrangian for point vortices on $\mathbb{S}^3$. By discretizing the Lagrangian variational principle on $\mathbb{S}^3$ (see Marsden and West [2001]), we will then be able to construct a variational integrator for point vortices which is automatically symplectic, second-order, and unit-length preserving.

Other approaches to the numerical integration of point vortices. Hamiltonian variational principles have been developed by Oh [1997] in the context of Floer homology and by Novikov [1982] for Morse theory (see also Cendra and Marsden [1987]). On the numerical front, geometrical numerical integration of Hamiltonian systems was described in Brown [2006], Ma and Rowley [2010] and Leok and Zhang [2011], but all of these references assume that the underlying symplectic manifold is exact. For non-exact symplectic forms (e.g. the case of point vortices on the sphere) it is as of yet not clear how to discretize the Hamiltonian variational principle so that the resulting numerical algorithms share some of the properties of the continuous system (such as symplecticity and momentum preservation). We do remark that Ma and Rowley [2010] perform a similar pullback as in this paper, but using the Lie algebra of the rotation group $SO(3)$ instead of the special unitary group $SU(2)$, in order to make the dynamics of point vortices on the sphere amenable to geometric integration.

2 The Hopf fibration

In this section, we introduce our notation and review some aspects of the geometry of the spheres $\mathbb{S}^2, \mathbb{S}^3$ and the Hopf fibration. This material is standard and can be found in any geometric physics textbook, for instance Frankel [2004]. More information about the Hopf fibration and its role in physics and geometry can be found in Montgomery [2002]; Urbantke [2003]; Lemaître [1948] and the references therein.

Notation. We will denote vectors in $\mathbb{C}^2$ and their Hermitian conjugates by

$$\varphi := \begin{bmatrix} z \\ u \end{bmatrix}, \quad \text{and} \quad \varphi^\dagger := \begin{bmatrix} z^*, & u^* \end{bmatrix},$$

where z^* is the complex conjugate of $z \in \mathbb{C}$. The Hermitian conjugate of a complex matrix A will be denoted by $A^\dagger$.

Lowercase Roman letters $a, b, \ldots$ will refer to the components φ^a of a vector φ in $\mathbb{C}^2$. The Greek letters $\alpha, \beta, \ldots$ will refer to the Cartesian components x^α of a vector $\mathbf{x} \in \mathbb{R}^3$. The imaginary unit will be denoted by i.

The Hermitian inner product on $\mathbb{C}^2$ is given by

$$\langle \varphi_1, \varphi_2 \rangle := \varphi_1^\dagger \varphi_2 = z_1^* z_2 + u_1^* u_2.$$

Note that the Euclidian inner product on $\mathbb{C}^2$ can be expressed as

$$\operatorname{Re} \langle \varphi_1, \varphi_2 \rangle = \operatorname{Re}(z_1^* z_2 + u_1^* u_2). \tag{2.1}$$

The geometry of $\mathbb{S}^2$. We think of the two-sphere $\mathbb{S}^2$ as the set of all unit-length vectors $\mathbf{x}$ in $\mathbb{R}^3$. The tangent plane $T_{\mathbf{x}}\mathbb{S}^2$ at an element $\mathbf{x} \in \mathbb{S}^2$ consists of all vectors, denoted by $\delta\mathbf{x} \in \mathbb{R}^3$, which are orthogonal to $\mathbf{x}$:

$$T_{\mathbf{x}}\mathbb{S}^2 = \{\delta\mathbf{x} \in \mathbb{R}^3 : \mathbf{x} \cdot \delta\mathbf{x} = 0\}.$$

In Cartesian coordinates, the area form Ω on $\mathbb{S}^2$ can be described as follows: Ω is the differential two-form given by

$$\Omega(\mathbf{x})(\delta\mathbf{x}, \delta\mathbf{y}) = \mathbf{x} \cdot (\delta\mathbf{x} \times \delta\mathbf{y}), \tag{2.2}$$

for all $\mathbf{x} \in \mathbb{S}^2$ and $\delta\mathbf{x}, \delta\mathbf{y} \in T_{\mathbf{x}}\mathbb{S}^2$. In spherical coordinates, $\Omega = \sin\theta d\theta \wedge d\phi$. Note that Ω is not exact.

The geometry of $\mathbb{S}^3$ and the group $SU(2)$. We let $\mathbb{S}^3$ be the unit sphere in $\mathbb{C}^2$:

$$\mathbb{S}^3 = \{(z, u) \in \mathbb{C}^2 : |z|^2 + |u|^2 = 1\}.$$

The tangent plane at an element $\varphi \in \mathbb{S}^3$ is given by the set of all vectors, denoted by $\delta\varphi \in \mathbb{C}^2$, which are orthogonal to φ:

$$T_\varphi \mathbb{S}^3 := \{\delta\varphi \in \mathbb{C}^2 : \operatorname{Re} \langle \delta\varphi, \varphi \rangle = 0\}, \tag{2.3}$$

where we have expressed the orthogonality between φ and $\delta\varphi$ using the inner product (2.1) in $\mathbb{C}^2$.

The unit sphere $\mathbb{S}^3$ can be embedded into the complex 2-by-2 matrices, by means of the mapping

$$\begin{bmatrix} z \\ u \end{bmatrix} \in \mathbb{S}^3 \mapsto \begin{bmatrix} z & -u^* \\ u & z^* \end{bmatrix} \in M_2(\mathbb{C}),$$

whose range is precisely the Lie group $SU(2)$ consisting of all Hermitian matrices ($U^\dagger = U$) with unit determinant ($\det U = 1$). The Lie algebra of $SU(2)$ is the vector space $\mathfrak{su}(2)$, consisting of all 2-by-2 matrices A which are anti-Hermitian ($A^\dagger = -A$) and traceless ($\operatorname{tr} A = 0$). The identification of $\mathbb{S}^3$ with $SU(2)$ provides a convenient description for the tangent spaces (2.3): we have that $\delta\varphi \in T_\varphi \mathbb{S}^3$ if and only if there is a matrix $A \in \mathfrak{su}(2)$ such that

$$\delta\varphi = A\varphi. \tag{2.4}$$

To see this, note that $A^\dagger = -A$ implies that $\langle \varphi, A\varphi \rangle$ is purely imaginary, so that $\operatorname{Re} \langle \varphi, A\varphi \rangle = 0$.

The Lie algebra $\mathfrak{su}(2)$ has dimension 3 and a convenient basis is given by the matrices $\tau_\alpha = \mathrm{i}\sigma_\alpha$, $\alpha = 1, 2, 3$, where the σ_α are the *Pauli spin matrices*:

$$\sigma_1 = \begin{bmatrix} 0 & 1 \\ 1 & 0 \end{bmatrix}, \quad \sigma_2 = \begin{bmatrix} 0 & -\mathrm{i} \\ \mathrm{i} & 0 \end{bmatrix}, \quad \text{and} \quad \sigma_3 = \begin{bmatrix} 1 & 0 \\ 0 & -1 \end{bmatrix}. \tag{2.5}$$

Given a matrix $A \in \mathfrak{su}(2)$, we will denote its components in this basis by a_α, $\alpha = 1, 2, 3$, and we put $\mathbf{a} := (a_1, a_2, a_3)$. Explicitly,

$$A = \mathbf{a} \cdot (\mathrm{i}\boldsymbol{\sigma}) = \sum_{\alpha=1}^{3} a_\alpha (\mathrm{i}\sigma_\alpha), \tag{2.6}$$

where $\boldsymbol{\sigma}$ represents the vector $(\sigma^1, \sigma^2, \sigma^3)$. We will refer to $\mathbf{a} \in \mathbb{R}^3$ as the *vector representation* of the matrix $A \in \mathfrak{su}(2)$.

The Pauli matrices satisfy a number of useful identities: the multiplication identity is

$$\sigma_\alpha \sigma_\beta = \delta_{\alpha\beta} I + \mathrm{i} \sum_{\gamma=1}^{3} \epsilon_{\alpha\beta\gamma} \sigma_\gamma, \tag{2.7}$$

for $\alpha, \beta = 1, 2, 3$, where I is the 2-by-2 unit matrix and $\epsilon_{\alpha\beta\gamma}$ the Levi-Civita permutation symbol. Secondly, there is the completeness property

$$\sum_{\alpha=1}^{3} (\sigma_\alpha)_{ab} (\sigma_\alpha)_{cd} = 2\delta_{ad}\delta_{bc} - \delta_{ab}\delta_{cd}, \tag{2.8}$$

for all $a, b, c, d = 1, 2$. Proofs of these identities can be found in any standard textbook on quantum mechanics.

The Hopf fibration. The group $U(1) \cong \mathbb{S}^1$ of unit complex numbers acts on $\mathbb{S}^3$ by the diagonal action: $e^{i\theta} \cdot (z, u) = (e^{i\theta} z, e^{i\theta} u)$ for all $e^{i\theta} \in \mathbb{S}^1$ and $(z, u) \in \mathbb{S}^3$. In terms of $SU(2)$-matrices, this action is described as

$$\begin{bmatrix} z & -u^* \\ u & z^* \end{bmatrix} \cdot e^{\mathrm{i}\theta} = \begin{bmatrix} z & -u^* \\ u & z^* \end{bmatrix} \begin{bmatrix} e^{\mathrm{i}\theta} & 0 \\ 0 & e^{-\mathrm{i}\theta} \end{bmatrix}. \tag{2.9}$$

The orbit space of this action, $\mathbb{S}^3/\mathbb{S}^1$, can be identified with the two-sphere $\mathbb{S}^2$. Explicitly, there exists a surjective submersion $\pi : \mathbb{S}^3 \to \mathbb{S}^2$, called the *Hopf fibration*, given by

$$\pi(z, u) = (2\,\mathrm{Re}(z^* u), 2\,\mathrm{Im}(z^* u), |z|^2 - |u|^2), \tag{2.10}$$

and the fibers of π coincide with the orbits of the group $\mathbb{S}^1$ in $\mathbb{S}^3$. In geometrical terms, the map $\pi : \mathbb{S}^3 \to \mathbb{S}^2$ makes $\mathbb{S}^3$ into the total space of a right principal fiber bundle with structure group $\mathbb{S}^1$ over $\mathbb{S}^2$. We will refer to the orbits of the $\mathbb{S}^1$-action (2.9) as the $\mathbb{S}^1$-*fibers* of $\mathbb{S}^3$.

The Hopf map can be expressed conveniently in terms of the Pauli matrices as follows. We let $\boldsymbol{\sigma}$ be the vector $(\sigma_1, \sigma_2, \sigma_3)$. The Hopf map (2.10) can then be described as

$$\pi(\varphi) = \varphi^\dagger \boldsymbol{\sigma} \varphi. \tag{2.11}$$

The right-hand side should be interpreted as a vector $\mathbf{x}$ in $\mathbb{R}^3$, whose components are given by $x^\alpha := \varphi^\dagger \sigma_\alpha \varphi$, $\alpha = 1, 2, 3$.

The inner product of two vectors $\mathbf{x}, \mathbf{y} \in \mathbb{R}^3$ can be given a convenient description using the Hopf map. Let $\mathbf{x} = \varphi^\dagger \boldsymbol{\sigma} \varphi$ and $\mathbf{y} = \psi^\dagger \boldsymbol{\sigma} \psi$. A straightforward consequence of (2.8) is then that

$$\mathbf{x} \cdot \mathbf{y} = 2(\varphi^\dagger \psi)(\psi^\dagger \varphi) - (\varphi^\dagger \varphi)(\psi^\dagger \psi). \tag{2.12}$$

Connection one-form and curvature. On $\mathbb{S}^3$, there is a distinguished one-form $\mathcal{A}$ which will play a crucial role in obtaining the Lagrangian formulation for point vortices. Explicitly, it is given by

$$\mathcal{A}(\varphi) = \mathrm{Im}(\varphi^\dagger \, \mathbf{d}\varphi),$$

and we denote the contraction of $\mathcal{A}(\varphi)$ with a vector $\dot{\varphi} = (\dot{z}, \dot{u})$ by

$$\mathcal{A}(\varphi) \cdot \dot{\varphi} = \mathrm{Im}(\varphi^\dagger \dot{\varphi}) = \mathrm{Im}(z^* \dot{z} + u^* \dot{u}). \tag{2.13}$$

Note the similarity between $\mathcal{A}$ and the one-form θ given in (1.4).

The form $\mathcal{A}$ is the connection one-form of a principal fiber bundle connection, but we will just treat it as a one-form. The curvature of $\mathcal{A}$ is given by

$$\mathbf{d}\mathcal{A} = \mathrm{Im}(\mathbf{d}\varphi^\dagger \wedge \mathbf{d}\varphi) = \mathrm{Im}(dz^* \wedge dz + du^* \wedge du),$$

and it can be shown that the area form Ω on $\mathbb{S}^2$, given by (2.2), satisfies

$$\pi^* \Omega = 2\mathbf{d}\mathcal{A}. \tag{2.14}$$

This result states that the two-form Ω, which is not exact, nevertheless becomes exact when pulled back along the Hopf map to $\mathbb{S}^3$. This will allow us to construct a linear Lagrangian for point vortices on $\mathbb{S}^3$.

3 Hamiltonian formulation of the vortex equations

In this section, we review the Hamiltonian description of the equations of motion (1.6) for point vortices on the unit sphere. This system of first-order ODEs can be written in Hamiltonian form, where the phase space is the Cartesian product $(\mathbb{S}^2)^N$ of N copies of the unit sphere $\mathbb{S}^2$, equipped with the symplectic form

$$\mathcal{B}_\Gamma(\mathbf{x}_1, \ldots, \mathbf{x}_N) = \sum_{i=1}^{N} \Gamma_i \Omega(\mathbf{x}_i), \tag{3.1}$$

where Ω is the standard symplectic area form on $\mathbb{S}^2$, given by (2.2).

The Hamiltonian function is given by

$$H = -\frac{1}{4\pi}\sum_{i<j}\Gamma_i\Gamma_j \log(2\sigma^2 + l_{ij}^2), \tag{3.2}$$

where $l_{ij} := \|\mathbf{x}_i - \mathbf{x}_j\|$ is the chord distance between the ith and the jth vortex and σ is the cutoff parameter introduced in (1.6).

Hamilton's equations are then given by $\mathbf{i}_{\dot{\mathbf{x}}}\mathcal{B}_\Gamma = \mathbf{d}H$. Explicitly, we are looking for a curve $t \mapsto \mathbf{x}(t) \in (\mathbb{S}^2)^N$ such that, for any variation $\delta\mathbf{x}(t) \in T_{\mathbf{x}(t)}(\mathbb{S}^2)^N$, we have that

$$\mathcal{B}_\Gamma(\dot{\mathbf{x}}, \delta\mathbf{x}) = \mathbf{d}H(\mathbf{x}) \cdot \delta\mathbf{x}.$$

Using the expression (2.2) for the symplectic form, this can be written as

$$\sum_{i=1}^N \Gamma_i \mathbf{x}_i(\dot{\mathbf{x}}_i \times \delta\mathbf{x}_i) = \sum_{i=1}^N \nabla_{\mathbf{x}_i} H(\mathbf{x}) \cdot \delta\mathbf{x}_i,$$

so that

$$\Gamma_i(\mathbf{x}_i \times \dot{\mathbf{x}}_i) = \nabla_{\mathbf{x}_i} H(\mathbf{x}) + \lambda_i \mathbf{x}_i, \tag{3.3}$$

where the Lagrange multipliers λ_i, $i = 1, \ldots, N$, have been introduced to enforce the constraint that the variations $\delta\mathbf{x}_i$ be tangent to the unit sphere, so that $\mathbf{x}_i \cdot \delta\mathbf{x}_i = 0$ for all $i = 1, \ldots, N$. Taking the cross product of (3.3) with $\mathbf{x}_i$ then results in

$$\Gamma_i(\mathbf{x}_i \times \dot{\mathbf{x}}_i) \times \mathbf{x}_i = \nabla_{\mathbf{x}_i} H(\mathbf{x}) \times \mathbf{x}_i,$$

and after expanding the double cross product and using the fact that $\|\mathbf{x}_i\| = 1$, we obtain

$$\Gamma_i \dot{\mathbf{x}}_i = \nabla_{\mathbf{x}_i} H(\mathbf{x}) \times \mathbf{x}_i, \tag{3.4}$$

which is equivalent to (1.6).

4 Lagrangian formulation of the vortex equations on $\mathbb{S}^3$

In this section, we show how the Hamiltonian equations (1.6) for point vortices can be given a Lagrangian formulation. To do this, we lift the point vortex system from the two-sphere $\mathbb{S}^2$ to the three-sphere $\mathbb{S}^3$ using the Hopf fibration.

Pullback of the Hamiltonian H. Using the projection π given in (2.10), we may pull back the Hamiltonian function on $\mathbb{S}^2$ to $\mathbb{S}^3$. If we denote the Hamiltonian function (3.2) by $H_{\mathbb{S}^2}$ and the pullback by $H_{\mathbb{S}^3}$, then we have that $H_{\mathbb{S}^3} = \pi^* H_{\mathbb{S}^2}$, or explicitly,

$$H_{\mathbb{S}^3}(\varphi_1, \ldots, \varphi_N) = H_{\mathbb{S}^2}(\pi(\varphi_1), \ldots, \pi(\varphi_N)), \tag{4.1}$$

for all $\varphi_1, \ldots, \varphi_N \in \mathbb{S}^3$. A straightforward computation shows that $H_{\mathbb{S}^3}$ is given by

$$H_{\mathbb{S}^3}(\varphi_1, \ldots, \varphi_N) := -\frac{1}{4\pi} \sum_{i<j} \Gamma_i \Gamma_j \log \left[2\sigma^2 + 4(1 - |\langle \varphi_i, \varphi_j \rangle|^2) \right]. \tag{4.2}$$

In the remainder, we will drop the subscript '$\mathbb{S}^3$' on the Hamiltonian function, denoting $H_{\mathbb{S}^3}$ simply as H. Note that H is invariant under multiplication by $e^{\mathrm{i}\theta} \in \mathbb{S}^1$ in each argument separately:

$$H(\ldots, e^{\mathrm{i}\theta}\varphi_k, \ldots) = H(\ldots, \varphi_k, \ldots), \tag{4.3}$$

for $k = 1, \ldots, N$. The infinitesimal version of this symmetry is

$$\frac{\partial H}{\partial \varphi_k} \varphi_k - \varphi_k^\dagger \frac{\partial H}{\partial \varphi_k^\dagger} = 0, \tag{4.4}$$

where there is *no sum over the index k*.

Since multiplying φ_k by a phase factor $e^{\mathrm{i}\theta}$ corresponds to moving along the $\mathbb{S}^1$-fiber through φ_k, we have that H depends only on the chord distance between the $\mathbb{S}^1$-fibers through $\varphi_1, \ldots, \varphi_N$. This can be shown explicitly in (4.2) by expressing the inner product $|\langle \varphi_i, \varphi_j \rangle|$ in terms of the Euclidian distance $\mathcal{D}(\varphi_i, \varphi_j)$ between the $\mathbb{S}^1$-fibers through φ_i and φ_j, where

$$\mathcal{D}(\varphi_i, \varphi_j) = 2(1 - |\langle \varphi_i, \varphi_j \rangle|).$$

The linear Lagrangian and the equations of motion. We now have all the elements to formulate a Lagrangian description for point vortices on $\mathbb{S}^3$. Recall that a linear Lagrangian has the general form $L = \Theta - H$, where $\mathbf{d}\Theta$ is the symplectic form. The symplectic structure on $(\mathbb{S}^3)^N$ is given by the pullback of the symplectic structure on $(\mathbb{S}^2)^N$,

$$\pi^* \left(\sum_{i=1}^N \Gamma_i \Omega_i \right) = \mathbf{d} \left(2 \sum_{i=1}^N \Gamma_i \mathcal{A}_i \right),$$

so it follows that $\Theta = 2\sum_{i=1}^N \Gamma_i \mathcal{A}_i$. Therefore, we obtain

$$L = 2 \sum_{i=1}^N \Gamma_i \mathcal{A}(\varphi_i) \cdot \dot{\varphi}_i - H(\varphi_1, \ldots, \varphi_N), \tag{4.5}$$

where $\varphi_i \in \mathbb{S}^3$ for $i = 1, \ldots, N$. This generalizes the expression (1.3) for the linear Lagrangian for point vortices in the plane.

The action functional is defined as

$$\mathcal{S}(\varphi(\cdot)) = \int_{t_0}^{t_1} L(\varphi(t), \dot{\varphi}(t)) dt, \tag{4.6}$$

where $\varphi(t) := (\varphi_1(t), \dots, \varphi_N(t))$ is a curve in $(\mathbb{S}^3)^N$ defined on the interval $[t_0, t_1]$, and its variation is given explicitly by

$$\delta\mathcal{S} = \sum_{i=1}^{N} \delta\varphi_i^\dagger \left(-2\mathrm{i}\Gamma_i \dot{\varphi}_i + \frac{\partial H}{\partial \varphi_i^\dagger} \right) + \sum_{i=1}^{N} \left(2\mathrm{i}\Gamma_i \dot{\varphi}_i^\dagger + \frac{\partial H}{\partial \varphi_i} \right) \delta\varphi_i, \tag{4.7}$$

where the infinitesimal variations $\delta\varphi_i$ and $\delta\varphi_i^\dagger$ need to be prescribed carefully. Since φ_i is an element of $\mathbb{S}^3$, the variations $\delta\varphi_i$ are elements of $T_\varphi\mathbb{S}^3$. Specifically, we have that $\delta\varphi_i$ is orthogonal to φ_i. This relation may be incorporated using Lagrange multipliers λ_i, resulting in the Euler–Lagrange equations

$$\boxed{2\mathrm{i}\Gamma_i \dot{\varphi}_i = \frac{\partial H}{\partial \varphi_i^\dagger} + \lambda_i \varphi_i,} \tag{4.8}$$

together with their Hermitian conjugates and the unit-length constraints

$$\langle \varphi_i, \varphi_i \rangle = 1. \tag{4.9}$$

This equation is the analogue of (1.1) for vortices on $\mathbb{S}^3$ and can be seen as a *nonlinear Schrödinger equation* on the product space $(\mathbb{S}^3)^N$. The analogy with (1.1) can be made more striking by interpreting φ_i as a *unit quaternion*, so that (4.8) becomes (up to a constant) the quaternionic version of the complex equation (1.1).

Determining the Lagrange multipliers. A curious feature of these equations is that the multipliers λ_i reflect *gauge degrees of freedom*, that is, any choice of λ_i will preserve the unit length constraint equally well. To see this, take the time derivative of (4.9) and substitute the equations of motion; the result is

$$\frac{1}{2\mathrm{i}\Gamma_i} \left(-\frac{\partial H}{\partial \varphi_i} - \lambda_i \varphi_i^\dagger \right) \varphi_i + \frac{1}{2\mathrm{i}\Gamma_i} \varphi_i^\dagger \left(\frac{\partial H}{\partial \varphi_i^\dagger} + \lambda_i \varphi_i \right) = 0,$$

which simplifies to

$$\frac{\partial H}{\partial \varphi_i} \varphi_i - \varphi_i^\dagger \frac{\partial H}{\partial \varphi_i^\dagger} = 0,$$

from which λ_i is absent. This expression is nothing but the infinitesimal symmetry relation (4.4) and is therefore identically satisfied.

With hindsight, it is not surprising that there is some indeterminacy in the solutions of (4.8). After all, these equations arise as pullbacks of equations on $\mathbb{S}^2$. From this point of view, changing the multipliers λ_i will change the dynamics in the direction of the $\mathbb{S}^1$-fibers, but will leave the horizontal dynamics (which projects down to $\mathbb{S}^2$) unchanged. This is similar to the *un-reduction approach* of Bruveris, Ellis, Holm, and Gay-Balmaz [2011], in which a complicated dynamical system on a manifold X is mapped into a simpler problem on the total space of a principal fiber bundle over X.

Relation with the equations on $(\mathbb{S}^2)^N$. By construction, the flow of the equations (4.8) on $(\mathbb{S}^3)^N$ will project down onto the flow of the point vortex equations (1.6) on $(\mathbb{S}^2)^N$. It is instructive, however, to see this explicitly.

We start again from the variational principle (4.7), but now we do not introduce a Lagrange multiplier to incorporate the unit-length constraint. For the sake of clarity, we suppress the explicit index i in (4.7) to arrive at

$$\delta\mathcal{S} = \delta\varphi^\dagger \left(-2\mathrm{i}\Gamma\dot{\varphi} + \frac{\partial H}{\partial \varphi^\dagger}\right) + \left(2\mathrm{i}\Gamma\dot{\varphi}^\dagger + \frac{\partial H}{\partial \varphi}\right)\delta\varphi. \tag{4.10}$$

As the variation $\delta\varphi$ is tangent to $\mathbb{S}^3$, it can be written as $\delta\varphi = A\varphi$, where $A \in \mathfrak{su}(2)$; see (2.4). Similarly, we have that $\delta\varphi^\dagger = \varphi^\dagger A^\dagger = -\varphi^\dagger A$. Upon substituting these expressions in (4.10), we arrive at

$$\begin{aligned}\delta\mathcal{S} &= -\varphi^\dagger A\left(-2\mathrm{i}\Gamma\dot{\varphi} + \frac{\partial H}{\partial \varphi^\dagger}\right) + \left(2\mathrm{i}\Gamma\dot{\varphi}^\dagger + \frac{\partial H}{\partial \varphi}\right)A\varphi \\ &= 2\,\mathrm{Re}\left[\left(2\mathrm{i}\Gamma\dot{\varphi}^\dagger + \frac{\partial H}{\partial \varphi}\right)A\varphi\right],\end{aligned}$$

so that $\delta\mathcal{S} = 0$ for all $A \in \mathfrak{su}(2)$ if and only if

$$\boxed{\mathrm{Re}\left[\left(2\mathrm{i}\Gamma\dot{\varphi}^\dagger + \frac{\partial H}{\partial \varphi}\right)\mathrm{i}\sigma_\alpha\varphi\right] = 0, \quad \alpha = 1,2,3,} \tag{4.11}$$

where the σ_α are the Pauli matrices (2.5). Note that these equations are equivalent to (4.8).

We now let $\mathbf{x} \in \mathbb{S}^2$ be the image of $\varphi \in \mathbb{S}^3$ under the Hopf map, and we recall from (2.11) that the components of $\mathbf{x}$ are given by $x_\alpha = \varphi^\dagger\sigma_\alpha\varphi$. Taking the time derivative, we obtain

$$\dot{x}_\alpha = 2\,\mathrm{Re}\left(\dot{\varphi}^\dagger\sigma_\alpha\varphi\right). \tag{4.12}$$

Similarly, we recall that the Hamiltonian functions $H_{\mathbb{S}^2}$ and $H_{\mathbb{S}^3}$ are related by (4.1), or explicitly $H_{\mathbb{S}^3}(\varphi,\varphi^\dagger) = H_{\mathbb{S}^2}(\varphi^\dagger\sigma_\alpha\varphi)$. Taking the derivative with respect to $\varphi^\dagger$ yields

$$\frac{\partial H_{\mathbb{S}^3}}{\partial\varphi} = \frac{\partial H_{\mathbb{S}^2}}{\partial x_\beta}\varphi^\dagger\sigma_\beta, \tag{4.13}$$

and a small calculation, involving the multiplication identity (2.7), then shows that

$$\mathrm{Re}\left[\mathrm{i}\frac{\partial H}{\partial\varphi}\sigma_\alpha\varphi\right] = \sum_{\beta,\gamma}\epsilon_{\alpha\beta\gamma}\frac{\partial H_{\mathbb{S}^2}}{\partial x_\beta}x_\gamma = (\nabla_{\mathbf{x}}H_{\mathbb{S}^2}\times\mathbf{x})_\alpha.$$

Substituting this expression and (4.12) into (4.11) then results in the following vector equations: $\Gamma\dot{\mathbf{x}} = \nabla_{\mathbf{x}}H_{\mathbb{S}^2}\times\mathbf{x}$, which, upon restoring the sum over all vortices, are nothing but the point vortex equations (3.4).

Intrinsic formulation of the point vortex equations. The point vortex equations (4.8) on $(\mathbb{S}^3)^N$ can be written in geometric form as follows. The point vortex trajectories are integral curves of a vector field Γ on $(\mathbb{S}^3)^N$, determined implicitly from the equation

$$\mathbf{i}_\Gamma \mathcal{B}_{\mathbb{S}_3} = \mathbf{d}H_{\mathbb{S}_3}, \tag{4.14}$$

where $\mathcal{B}_{\mathbb{S}_3}$ is the pullback to $(\mathbb{S}^3)^N$ of the point vortex symplectic form $\mathcal{B}$ given in (3.1): $\mathcal{B}_{\mathbb{S}_3} = \pi^*\mathcal{B}$, with $\pi : \mathbb{S}^3 \to \mathbb{S}^2$ the Hopf map. This makes it clear that the equations (4.8) do not determine the dynamics completely: we may add to the solution Γ of (4.14) any π-vertical vector field without changing the projected dynamics.

We may resolve this indeterminacy by replacing $\mathbb{S}^3$ by its *symplectification*, which is the product manifold $\mathbb{S}^3 \times \mathbb{R}^+$ equipped with the symplectic form

$$\tilde{\mathcal{B}} = \mathbf{d}(r\mathcal{A}),$$

where r is the coordinate on the $\mathbb{R}^+$-factor. The motion of point vortices on this twice-enlarged space projects down to the motion of point vortices on $\mathbb{S}^2$, and can be viewed, paraphrasing the terminology of Kostant [2005], as a version of "prequantum vortex dynamics."[1]

5 Variational integrators on $SU(2)^N$

In this section, we propose a discrete version of the point vortex equations on $(\mathbb{S}^3)^N$. We begin by discretizing the linear Lagrangian (4.5) using centered finite differences. By taking discrete variations, we then obtain a discrete version of the equations (4.8) where the constraints are enforced using a Lagrange multiplier. These equations can be seen as a version of the Moser-Veselov equations (see Moser and Veselov [1991]) on $(\mathbb{S}^3)^N$.

By projecting onto the annihilator space of the constraint forces, we then obtain a discrete version of the projected equations (4.11). Finally, we use the isomorphism between $\mathbb{S}^3$ and $SU(2)$ to write the discrete equations of motion in the form of a Lie group variational integrator (see Lee, Leok, and McClamroch [2007]) on $SU(2)$ and we argue that this form of the equations is especially well-suited for numerical implementation.

5.1 Discrete Lagrangian and discrete equations of motion

Let M be the number of discrete time steps, with constant time increment $h > 0$, and denote the variables at time $t_n := nh$ by $\varphi^n := (\varphi_1^n, \ldots, \varphi_N^n) \in (\mathbb{S}^3)^N$. We now propose a discrete counterpart of the linear Lagrangian L in (4.5) by approximating the action functional (4.6) over the interval $[t_n, t_{n+1}]$ by using piecewise linear

[1] We thank M. Gotay for bringing this point to our attention.

interpolants and the midpoint rule (see Marsden and West [2001]). In this way, we construct a discrete Lagrangian $L_d : (\mathbb{S}^3)^N \times (\mathbb{S}^3)^N \to \mathbb{R}$ of the form

$$L_d(\varphi^n, \varphi^{n+1}) = hL\left(\frac{\varphi^n + \varphi^{n+1}}{2}, \frac{\varphi^{n+1} - \varphi^n}{h}\right). \tag{5.1}$$

Explicitly, the discrete linear Lagrangian is given by

$$L_d(\varphi^n, \varphi^{n+1}) = 2\sum_{i=1}^{N} \Gamma_i \mathcal{A}(\varphi_i^{n+1/2}) \cdot (\varphi_i^{n+1} - \varphi_i^n) + hH(\varphi^{n+1/2}), \tag{5.2}$$

where $\varphi^{n+1/2} := (\varphi^n + \varphi^{n+1})/2$.

The discrete action sum is now defined as

$$\mathcal{S}_d(\varphi^1, \ldots, \varphi^M) = \sum_{i=1}^{M-1} L_d(\varphi^n, \varphi^{n+1}),$$

and taking variations with respect to φ_i^n and $(\varphi_i^n)^\dagger$ yields

$$\delta\mathcal{S}_d = \sum_{k=1}^{N}\sum_{n=1}^{M-1} \delta(\varphi_k^n)^\dagger \Big[-\mathrm{i}\Gamma_k\left(\varphi_k^{n+1} - \varphi_k^{n-1}\right) - h\lambda_k^n \varphi_k^n + \frac{h}{2}\left(D_{\varphi_k^\dagger} H(\varphi^{n-1/2}) + D_{\varphi_k^\dagger} H(\varphi^{n+1/2})\right)\Big] + (\text{c.c.}), \tag{5.3}$$

where "(c.c.)" stands for the complex conjugate of the previous expression. The discrete Euler–Lagrange equations are hence

$$\boxed{-\mathrm{i}\Gamma_k\left(\varphi_k^{n+1} - \varphi_k^{n-1}\right) + \frac{h}{2}\left(D_{\varphi_k^\dagger} H(\varphi^{n-1/2}) + D_{\varphi_k^\dagger} H(\varphi^{n+1/2})\right) - h\lambda_k^n \varphi_k^n = 0,} \tag{5.4}$$

together with their Hermitian conjugates and the unit-length constraints

$$\left\langle \varphi_i^{n+1}, \varphi_i^{n+1} \right\rangle = 1, \tag{5.5}$$

and can be viewed as the discrete analogues of the continuous equations (4.8).

In contrast to the continuous case, the Lagrange multipliers λ_k^n in (5.4) are no longer arbitrary. Instead, they can be found by substituting the discrete equations of motion into the unit-length constraint (5.5) and solving the resulting system of quadratic equations for λ_k^n.

Other discretizations. Instead of the midpoint quadrature formula, leading to the discrete Lagrangian (5.1), we could have chosen another approximation for the discrete Lagrangian, leading to a different set of discrete equations. Although these equations formally exhibit the same properties (symplecticity, preservation of the unit length constraint, etc.) as the midpoint method introduced previously, some of them suffer from undesirable side-effects. A particularly revealing example is

obtained by using the trapezoid rule instead of the midpoint rule, leading to the discrete Lagrangian

$$L_d(\varphi^n, \varphi^{n+1}) = \frac{h}{2}\left(L\left(\varphi^n, \frac{\varphi^{n+1}-\varphi^n}{h}\right) + L\left(\varphi^{n+1}, \frac{\varphi^{n+1}-\varphi^n}{h}\right)\right),$$

which gives rise to the discrete Euler–Lagrange equations

$$-\mathrm{i}\Gamma_k\left(\varphi_k^{n+1} - \varphi_k^{n-1}\right) + hD_{\varphi_k^\dagger}H(\varphi^n) = h\lambda_k^n\varphi_k^n, \tag{5.6}$$

together with unit-length constraints (5.5). This system, however, is equivalent to the 2-step symmetric explicit midpoint integrator (see Hairer, Lubich, and Wanner [2002, Sec. XV.3.2]), which is well-known to exhibit parasitic solutions which grow linearly in time. The same observation is true for the integrator of Rowley and Marsden [2002] with $\sigma = 0$ or 1;[2] see appendix A for details.

5.2 The projected midpoint equations

It is possible to obtain an equivalent version of the equations (5.4) which does not involve the Lagrange multipliers λ_k^n. To this end, we return to the discrete variational principle (5.3). As in the case of the continuous variational principle, we again suppress the vortex index k to arrive at

$$\delta\mathcal{S}_d = \sum_{n=1}^{M-1} \delta(\varphi^n)^\dagger\left[-\mathrm{i}\Gamma\left(\varphi^{n+1}-\varphi^{n-1}\right) + \frac{h}{2}\left(D_{\varphi^\dagger}H(\varphi^{n-1/2}) + D_{\varphi^\dagger}H(\varphi^{n+1/2})\right)\right] + (\text{c.c.}).$$

Instead of introducing a Lagrange multiplier to enforce the unit-length constraint, we impose the condition that the variations $\delta\varphi$ and $\delta\varphi^\dagger$ are tangent to the sphere, so that they can be written as

$$\delta\varphi = A\varphi, \quad \text{and} \quad \delta\varphi^\dagger = -\varphi^\dagger A,$$

where $A \in \mathfrak{su}(2)$ is arbitrary; see (2.4). Proceeding as in the case of the continuous variational principle, we then arrive at the following discrete equations:

$$\boxed{\mathrm{Re}\left[(\varphi^n)^\dagger(\mathrm{i}\sigma_\alpha)\left(-\mathrm{i}\Gamma\left(\varphi^{n+1}-\varphi^{n-1}\right) + \frac{h}{2}\left(D_{\varphi^\dagger}H(\varphi^{n-1/2}) + D_{\varphi^\dagger}H(\varphi^{n+1/2})\right)\right)\right] = 0,} \tag{5.7}$$

for $\alpha = 1, 2, 3$. These equations are supplemented by the unit-length constraint (5.5). Note that the equations (5.7) are the discrete version of the continuous projected vortex equations (4.11). Another, more direct way to arrive at these equations is simply to project the discrete Euler–Lagrange equations (5.4) onto the subspace orthogonal to φ^n.

[2] Here σ refers to the interpolation parameter used in Rowley and Marsden [2002], and should not be confused with the cutoff parameter used in the rest of the current paper.

The equivalent first-order system. The equations (5.7) are second-order discrete equations: given $(\varphi^{n-1}, \varphi^n)$, the equations can be solved to find φ^{n+1}. The discrete equations of motion are hence not self-starting: given the initial positions φ^0 for the point vortices, a standard one-step integrator needs to be used to find the positions φ^1 at the intermediate time $t_1 = h$. Afterwards, the discrete equations of motion can be used to integrate the system forwards in time.

We now present a way to circumvent this problem by writing the two-step method (5.7) as the composition of two one-step methods, which are obviously self-starting. That this decomposition is possible is a consequence of the fact that the Lagrangian (4.5) is linear in the velocities, and will be analyzed further in Appendix A. For now, we just focus on the computations for the point vortex equations.

We first write the equations (5.7) as

$$\operatorname{Re}\left[(\varphi^n)^\dagger(\mathrm{i}\sigma_\alpha)\left(-\mathrm{i}\Gamma(\varphi^{n+1}-\varphi^n)+\frac{h}{2}D_{\varphi^\dagger}H(\varphi^{n+1/2})\right)\right] = -d_\alpha^n, \tag{5.8}$$

where d_α^n depends on the configurations φ^n and φ^{n-1} only:

$$d_\alpha^n := \operatorname{Re}\left[(\varphi^n)^\dagger(\mathrm{i}\sigma_\alpha)\left(-\mathrm{i}\Gamma(\varphi^{n}-\varphi^{n-1})+\frac{h}{2}D_{\varphi^\dagger}H(\varphi^{n-1/2})\right)\right]. \tag{5.9}$$

We now focus on the left-hand side of (5.8), which we solve for φ^{n+1}: we introduce a map $\Phi_h : \mathbb{S}^3 \to \mathbb{S}^3$ defined by the property that $\Phi_h(\varphi^n) = \varphi^{n+1}$ if and only if the left-hand side of (5.8) vanishes:

$$\operatorname{Re}\left[(\varphi^n)^\dagger(\mathrm{i}\sigma_\alpha)\left(-\mathrm{i}\Gamma(\varphi^{n+1}-\varphi^n)+\frac{h}{2}D_{\varphi^\dagger}H(\varphi^{n+1/2})\right)\right] = 0. \tag{5.10}$$

Now, the *adjoint* of Φ_h is the map $\Phi_h^* : \mathbb{S}^3 \to \mathbb{S}^3$ defined by

$$\Phi_h^*(\varphi^{n-1}) = \varphi^n \quad \text{if and only if} \quad \Phi_{-h}(\varphi^n) = \varphi^{n-1}.$$

A small calculation then shows that Φ_h^* is implicitly determined by the left-hand side of (5.9). In other words, $\Phi_h^*(\varphi^{n-1}) = \varphi^n$ if and only if

$$\operatorname{Re}\left[(\varphi^n)^\dagger(\mathrm{i}\sigma_\alpha)\left(-\mathrm{i}\Gamma(\varphi^{n}-\varphi^{n-1})+\frac{h}{2}D_{\varphi^\dagger}H(\varphi^{n-1/2})\right)\right] = 0. \tag{5.11}$$

A possible way of solving the second-order equations (5.7) is therefore as follows. Starting from an arbitrary element $\varphi^{n-1} \in \mathbb{S}^3$ we apply alternatingly the adjoint map to obtain $\varphi^n = \Phi_h^*(\varphi^{n-1})$, and the direct map Φ_h to obtain $\varphi^{n+1} = \Phi_h(\varphi^n)$. By the previous calculation, the resulting triple $(\varphi^{n-1}, \varphi^n, \varphi^{n+1})$ is then a solution of (5.7). We summarize this in the following proposition.

Proposition 5.1. *Let $\varphi^{n-1} \in \mathbb{S}^3$ and put $\varphi^n = \Phi_h^*(\varphi^{n-1})$ and $\varphi^{n+1} = \Phi_h(\varphi^n)$. The triple $(\varphi^{n-1}, \varphi^n, \varphi^{n+1})$ is then a solution of the discrete second-order equations (5.7).*

The maps Φ_h and Φ_h^* both approximate the continuous flow, but it can be checked that they are only first-order accurate. It is only their composition $\Phi_h \circ \Phi_h^*$ that is symmetric and hence second-order accurate.

Note also that this decomposition gives us only a subset of all the solutions of the discrete second-order equations (5.7). For instance, if we start from $(\varphi^{n-1}, \varphi^n) \in \mathbb{S}^3 \times \mathbb{S}^3$ such that φ^n is only approximately equal to $\Phi_h^*(\varphi^{n-1})$, then $(\varphi^{n-1}, \varphi^n)$ will satisfy (5.9) for a non-zero value of d_α^n. However, we can then solve (5.8) for φ^{n+1} using that d_α^n as the right-hand side. The constants d_α^n can now be incorporated in the definition of the first-order maps Φ_h, Φ_h^*, so that solving (5.7) is equivalent to taking one step with the first-order map and one step with its adjoint. From this point of view, d_α^n becomes a slack variable. In practice, this will not be an issue, since we mostly just start from the initial positions φ^0 of the point vortices and then solve for φ^1 using (5.11), so that $d_\alpha^n = 0$.

5.3 Implementing the unit-length constraint: the Cayley map

When we solve (5.10) for φ^{n+1}, we still need to impose the unit-length constraint (5.5). This can be done conveniently using the geometry of $SU(2)$: we write the update map $\varphi^n \mapsto \varphi^{n+1}$ as

$$\varphi^{n+1} = U^{(n)} \varphi^n,$$

where $U^{(n)}$ is an element of $SU(2)$. This ensures that the length of φ^n stays constant over time, since

$$(\varphi^{n+1})^\dagger \varphi^{n+1} = (\varphi^n)^\dagger (U^{(n)})^\dagger U^{(n)} \varphi^n = (\varphi^n)^\dagger \varphi^n,$$

so that, in particular, $\|\varphi^n\| = 1$ implies that $\left\|\varphi^{n+1}\right\| = 1$.

The equations (5.10) for φ^{n+1} can now be expressed as

$$\operatorname{Re}\left[(\varphi^n)^\dagger (\mathrm{i}\sigma_\alpha)\left(-\mathrm{i}\Gamma(U^{(n)} - I_{2\times 2})\varphi^n + \frac{h}{2} D_{\varphi^\dagger} H(\varphi^{n+1/2})\right)\right] = 0. \tag{5.12}$$

These equations can be solved for $U^{(n)}$ directly, but a computationally more advantageous approach is as follows. As long as the step size h is small, the update matrix $U^{(n)}$ will be in a neighborhood of the identity element in $SU(2)$. We now parametrize that neighborhood by means of the *Cayley transform* $\operatorname{Cay} : \mathfrak{su}(2) \to SU(2)$, given by

$$\operatorname{Cay}(A) = (I + A)(I - A)^{-1}.$$

That is, we search for an element $A^{(n)} \in \mathfrak{su}(2)$ such that $U^{(n)} = \operatorname{Cay}(A^{(n)})$ will solve (5.12). The advantage is that $\mathfrak{su}(2)$ is a linear space, and that no constraints need to be imposed on $A^{(n)}$, as the range of the Cayley map is automatically contained within $SU(2)$. A standard nonlinear solver can therefore be used to find $A^{(n)}$.

Computational savings. Significant computational savings can be obtained by rewriting the Cayley map in a more convenient form. We recall from (2.6) that $\mathfrak{su}(2)$ is isomorphic with $\mathbb{R}^3$, and we denote the vector representation of $A^{(n)}$ by $\mathbf{a}^{(n)} \in \mathbb{R}^3$. A small calculation then shows that the Cayley transform can be expressed as

$$U^{(n)} = \mathrm{Cay}(A^{(n)}) = \frac{1}{1 + \left\|\mathbf{a}^{(n)}\right\|^2} \left((1 - \|\mathbf{a}^{(n)}\|^2) I + 2A^{(n)} \right), \tag{5.13}$$

so that

$$U^{(n)} - I_{2\times 2} = \frac{2}{1 + \|\mathbf{a}^{(n)}\|^2} \left(A^{(n)} - \|\mathbf{a}^{(n)}\|^2 I_{2\times 2} \right).$$

The terms proportional to Γ in (5.12) can then be written as

$$\begin{aligned} \mathrm{Re}\left[\Gamma(\varphi^n)^\dagger \sigma_\alpha (U^{(n)} - I_{2\times 2})\varphi^n\right] &= \frac{2\Gamma}{1 + \left\|\mathbf{a}^{(n)}\right\|^2} \mathrm{Re}\left[(\varphi^n)^\dagger \sigma_\alpha (A^{(n)} - \|\mathbf{a}^{(n)}\|^2 I_{2\times 2})\varphi^n\right] \\ &= \frac{2\Gamma}{1 + \left\|\mathbf{a}^{(n)}\right\|^2} \left(\mathrm{Re}\left[(\varphi^n)^\dagger \sigma_\alpha A^{(n)} \varphi^n\right] - \|\mathbf{a}^{(n)}\|^2 \mathrm{Re}\left[(\varphi^n)^\dagger \sigma_\alpha \varphi^n\right] \right) \\ &= \frac{-2\Gamma}{1 + \left\|\mathbf{a}^{(n)}\right\|^2} (\mathbf{a}^{(n)} \times \mathbf{x}^{(n)} + \|\mathbf{a}^{(n)}\|^2 \mathbf{x}^{(n)})_\alpha, \end{aligned} \tag{5.14}$$

where we have used the expression (2.11) for the Hopf fibration to write $x^n_\alpha = (\varphi^n)^\dagger \sigma^\alpha \varphi^n$, as well as the identity

$$\begin{aligned} (\varphi^n)^\dagger \sigma_\alpha A^{(n)} \varphi^n &= \mathrm{i} \sum_{\beta=1}^{3} (\mathbf{a}^{(n)})_\beta (\varphi^n)^\dagger \sigma_\alpha \sigma_\beta \varphi^n \\ &= \mathrm{i}(\mathbf{a}^{(n)})_\alpha - (\mathbf{a}^{(n)} \times \mathbf{x}^{(n)})_\alpha, \end{aligned}$$

which follows easily from (2.7).

Similarly, the terms in (5.12) involving the derivatives of the Hamiltonian can be written using (4.13) as

$$\begin{aligned} &\mathrm{Re}\left((\varphi^n)^\dagger (\mathrm{i}\sigma_\alpha) D_{\varphi^\dagger} H(\varphi^{n+1/2}) \right) = \\ &\quad \frac{1}{1 + \|\mathbf{a}_n\|^2} \left(\mathbf{x}^n \times \nabla H^{n+1/2}_{\mathbb{S}^2} - (\mathbf{a}^n \cdot \mathbf{x}^n) \nabla H^{n+1/2}_{\mathbb{S}^2} - (\mathbf{a}^n \times \mathbf{x}^n) \times \nabla H^{n+1/2}_{\mathbb{S}^2} \right)_\alpha, \end{aligned}$$

where $H_{\mathbb{S}^2}$ is the original point vortex Hamiltonian (3.2).

Combining this expression with (5.14), we get that the first-order equations (5.12) for $U^{(n)}$ are equivalent to the following nonlinear equation for $\mathbf{a}^{(n)}$:

$$\begin{aligned} &\frac{4\Gamma}{h} (\mathbf{a}^{(n)} \times \mathbf{x}^{(n)} + \|\mathbf{a}^{(n)}\|^2 \mathbf{x}^{(n)}) = \\ &\qquad \mathbf{x}^{(n)} \times \nabla H^{n+1/2}_{\mathbb{S}^2} - (\mathbf{a}^{(n)} \cdot \mathbf{x}^{(n)}) \nabla H^{n+1/2}_{\mathbb{S}^2} - (\mathbf{a}^{(n)} \times \mathbf{x}^{(n)}) \times \nabla H^{n+1/2}_{\mathbb{S}^2}. \end{aligned} \tag{5.15}$$

While this equation looks considerably more complicated than the original equation (5.12), it can in fact be reduced to a system of easier equations, described in the following proposition. To set the notation, we decompose $\mathbf{a}^{(n)}$ into a part $\mathbf{a}_\perp^{(n)}$ perpendicular to $\mathbf{x}^{(n)}$, and a part $\mu\mathbf{x}^{(n)}$ along $\mathbf{x}^{(n)}$:

$$\mathbf{a}^{(n)} = \mathbf{a}_\perp^{(n)} + \mu\mathbf{x}^{(n)}. \tag{5.16}$$

Proposition 5.2. *There are two distinct sets of solutions for the direct first-order equation (5.15), depending on the value of μ:*

1. *For the first class of solutions, $\mu = 0$ and $\mathbf{a}^{(n)} = \mathbf{a}_\perp^{(n)}$ satisfies*

$$\frac{4\Gamma}{h}\mathbf{a}^{(n)} = \mathbf{x}^{(n)} \times (\mathbf{x}^{(n)} \times \nabla H^{n+1/2}) + (\mathbf{x}^{(n)} \cdot \nabla H^{n+1/2})\mathbf{x}^{(n)} \times \mathbf{a}^{(n)}. \tag{5.17}$$

2. *For the second class of solutions,*

$$\mu = -\frac{h}{4\Gamma}(\mathbf{x}^{(n)} \cdot \nabla H^{n+1/2} + \mathbf{a}_\perp^{(n)} \cdot (\nabla H^{n+1/2} \times \mathbf{x}^{(n)})). \tag{5.18}$$

Substituting (5.16) and (5.18) into (5.15) yields an implicit equation for $\mathbf{a}_\perp^{(n)}$.

Proof. To simplify the notation, we omit the superscripts '(n)' from the quantities involved, and we denote the gradient of the Hamiltonian simply by ∇H. In this way, (5.15) becomes

$$\frac{4\Gamma}{h}(\mathbf{a} \times \mathbf{x} + \|\mathbf{a}\|^2\mathbf{x}) = \mathbf{x} \times \nabla H - (\mathbf{a} \cdot \mathbf{x})\nabla H - (\mathbf{a} \times \mathbf{x}) \times \nabla H, \tag{5.19}$$

to be solved for $\mathbf{a}$. We substitute the decomposition (5.16) into this equation to obtain

$$\frac{4\Gamma}{h}(\mathbf{a}_\perp \times \mathbf{x} + \|\mathbf{a}\|^2\mathbf{x}) = \mathbf{x} \times \nabla H - \mu\nabla H - (\mathbf{a}_\perp \times \mathbf{x}) \times \nabla H, \tag{5.20}$$

where we have used the fact that $\mathbf{x}^2 = 1$. Taking the dot product with $\mathbf{x}$ gives

$$\frac{4\Gamma}{h}\|\mathbf{a}\|^2 = -\mu(\mathbf{x} \cdot \nabla H) - \mathbf{a}_\perp \cdot \nabla H. \tag{5.21}$$

Taking the cross product of (5.20) with $\mathbf{x}$ results in

$$-\frac{4\Gamma}{h}\mathbf{a}_\perp = (\mathbf{x} \times \nabla H) \times \mathbf{x} - \mu(\nabla H \times \mathbf{x}) + (\mathbf{x} \cdot \nabla H)(\mathbf{a}_\perp \times \mathbf{x}). \tag{5.22}$$

We now take the dot product of this equation with $\mathbf{a}_\perp$ to get

$$-\frac{4\Gamma}{h}\|\mathbf{a}_\perp\|^2 = \mathbf{a}_\perp \cdot \nabla H - \mu\mathbf{a}_\perp \cdot (\nabla H \times \mathbf{x}),$$

and we subtract this equation from (5.21) to obtain the following quadratic equation for μ:

$$\frac{4\Gamma}{h}\mu^2 + \mu(\mathbf{x} \cdot \nabla H + \mathbf{a}_\perp \cdot (\nabla H \times \mathbf{x})) = 0,$$

the solutions of which are $\mu = 0$ and μ given by (5.18). When $\mu = 0$, $\mathbf{a} = \mathbf{a}_\perp$, and (5.22) simplifies to (5.17). ■

We stress that the solution for $\mu \neq 0$ is as valid from a physical point of view as the solution for $\mu = 0$, and there is a priori no reason to choose one over the other. In fact, we will see that consistently choosing the solution with $\mu \neq 0$ results in a different numerical algorithm, which we have termed the *μ-Hopf integrator*, which has the same good properties (symplecticity, second-order accuracy) as the integrator obtained by choosing $\mu = 0$. We will present a numerical comparison between both integrators at the end of Section 6.1 but for now we choose the solution corresponding to $\mu = 0$ in proposition 5.2, as it gives rise to a simpler equation for $\mathbf{a}^{(n)}$.

The adjoint equations. Having reduced the direct first-order equations (5.10) to a nonlinear equation on the Lie algebra $\mathfrak{su}(2)^N$, we now turn to the adjoint first-order equations (5.11). For these equations, we write the update map as

$$\varphi^{(n)} = U^{(n-1)}\varphi^{(n-1)}, \tag{5.23}$$

so that

$$\varphi^{(n-1)} = (U^{(n-1)})^\dagger \varphi^{(n)},$$

and we substitute this into (5.11) to get

$$\mathrm{Re}\left[(\varphi^n)^\dagger(\mathrm{i}\sigma_\alpha)\left(-\mathrm{i}\Gamma((U^{(n-1)})^\dagger - I_{2\times 2})\varphi^n - \frac{h}{2}D_{\varphi^\dagger}H(\varphi^{n+1/2})\right)\right] = 0, \tag{5.24}$$

which is very similar to (5.12): to obtain (5.24) from (5.12), we just have to make the substitution

$$U^{(n)} \mapsto (U^{(n-1)})^\dagger, \quad h \mapsto -h.$$

Using the Cayley map, we now write

$$U^{(n-1)} = \mathrm{Cay}(A^{(n-1)}), \quad \text{so that} \quad (U^{(n-1)})^\dagger = \mathrm{Cay}(-A^{(n-1)}),$$

where the matrix $A^{(n-1)}$, or rather its vector form $\mathbf{a}^{(n-1)}$, satisfies the following equation:

$$\begin{aligned} &-\frac{4\Gamma}{h}(-\mathbf{a}^{(n-1)} \times \mathbf{x}^{(n)} + \|\mathbf{a}^{(n-1)}\|^2\mathbf{x}^{(n)}) = \\ &\mathbf{x}^{(n)} \times \nabla H_{\mathbb{S}^2}^{n-1/2} + (\mathbf{a}^{(n-1)} \cdot \mathbf{x}^{(n)})\nabla H_{\mathbb{S}^2}^{n-1/2} + (\mathbf{a}^{(n-1)} \times \mathbf{x}^{(n)}) \times \nabla H_{\mathbb{S}^2}^{n-1/2}, \end{aligned} \tag{5.25}$$

which was obtained from (5.15) by making the substitution $\mathbf{a}^{(n)} \mapsto -\mathbf{a}^{(n-1)}$ and $h \mapsto -h$. Note that in the above, $\mathbf{x}^{(n)}$ depends on $\mathbf{a}^{(n-1)}$:

$$\mathbf{x}^{(n)} = \pi(\varphi^{(n)}) = \pi\left(U^{(n-1)}\varphi^{(n-1)}\right) = \pi\left(\mathrm{Cay}(A^{(n-1)})\varphi^{(n-1)}\right), \tag{5.26}$$

where $\varphi^{(n-1)}$ is given and $A^{(n-1)} \in \mathfrak{su}(2)$ is the matrix form of $\mathbf{a}^{(n-1)} \in \mathbb{R}^3$. The adjoint equations will therefore be computationally somewhat more expensive to solve than the direct equations, since now $\mathbf{x}^{(n)}$ also depends on the Lie algebra element $\mathbf{a}^{(n-1)}$.

The solutions of the equations (5.25) can now be described by the following proposition:

Proposition 5.3. *There are two distinct sets of solutions for the adjoint first-order equation (5.25), depending on the value of μ:*

1. *For the first class of solutions, $\mu = 0$ and $\mathbf{a}^{(n-1)} = \mathbf{a}_\perp^{(n-1)}$ satisfies*

$$-\frac{4\Gamma}{h}\mathbf{a}^{(n-1)} = \mathbf{x}^{(n)} \times (\mathbf{x}^{(n)} \times \nabla H^{n-1/2}) - (\mathbf{x}^{(n)} \cdot \nabla H^{n-1/2})\mathbf{x}^{(n)} \times \mathbf{a}^{(n-1)}.$$

2. *For the second class of solutions,*

$$\mu = \frac{h}{4\Gamma}(\mathbf{x}^{(n)} \cdot \nabla H^{n-1/2} - \mathbf{a}_\perp^{(n-1)} \cdot (\nabla H^{n-1/2} \times \mathbf{x}^{(n)})).$$

Substituting this and $\mathbf{a}^{(n-1)} = \mathbf{a}_\perp^{(n-1)} + \mu\mathbf{x}^{(n)}$ into (5.25) yields an implicit equation for $\mathbf{a}_\perp^{(n-1)}$.

In both cases, $\mathbf{x}^{(n)}$ depends on $\mathbf{a}^{(n-1)}$ and is found from $\mathbf{x}^{(n-1)}$ using (5.26).

Again, we will focus from this point on the solution with $\mu = 0$, even though the other solution is also physically admissible. See the last part of Section 6.1 for a more in-depth discussion.

5.4 Computational algorithm

We now summarize the developments of the previous sections to arrive at the following numerical algorithm. We restore the index $k = 1, \dots, N$ labeling the individual vortices. Given initial conditions φ_k^{n-1}, $k = 1, \dots, N$ for the point vortices, apply the following algorithm:

1. For each point vortex, find $\mathbf{a}_k^{(n-1)} \in \mathbb{R}^3$ by solving the *adjoint equation*:

$$-\frac{4\Gamma}{h}\mathbf{a}_k^{(n-1)} = \mathbf{x}_k^{(n)} \times (\mathbf{x}_k^{(n)} \times \nabla H^{n+1/2}) - (\mathbf{x}_k^{(n)} \cdot \nabla H^{n+1/2})\mathbf{x}_k^{(n)} \times \mathbf{a}_k^{(n-1)}. \quad (5.27)$$

   Here $\mathbf{x}_k^{(n)}$ depends on $\mathbf{a}_k^{(n-1)}$ and $\varphi_k^{(n-1)}$ through (5.26).

2. Let $\varphi_k^{(n)} = \mathrm{Cay}(\mathbf{a}_k^{(n-1)})\varphi_k^{(n-1)}$ and put $\mathbf{x}_k^{(n)} = \pi(\varphi_k^{(n)})$.

3. For each point vortex, find $\mathbf{a}_k^{(n)} \in \mathbb{R}^3$ by solving the *direct equation*:

$$\frac{4\Gamma}{h}\mathbf{a}_k^{(n)} = \mathbf{x}_k^{(n)} \times (\mathbf{x}_k^{(n)} \times \nabla H^{n+1/2}) + (\mathbf{x}_k^{(n)} \cdot \nabla H^{n+1/2})\mathbf{x}_k^{(n)} \times \mathbf{a}_k^{(n)}. \quad (5.28)$$

4. Let $\varphi_k^{(n+1)} = \mathrm{Cay}(\mathbf{a}_k^{(n)})\varphi_k^{(n)}$ and put $\mathbf{x}_k^{(n+1)} = \pi(\varphi_k^{(n+1)})$.

5. Repeat.

As we shall see below, the resulting flow is second-order accurate, symplectic, and preserves the unit-length constraint by construction. The advantage of using this version of the discrete equations of motion rather than the original formulations (5.4) or (5.7) is that the equations (5.27) and (5.28) for $\mathbf{a}^{(n-1)}$ and $\mathbf{a}^{(n)}$ are defined on $\mathfrak{su}(2)^N$, a linear space, and hence can be solved using a standard nonlinear solver. We stress, however, that these equations are equivalent to the original discrete equations of motion defined directly on $(\mathbb{S}^3)^N$.

Properties of the variational integrator. Since we have started from the midpoint discretization of a continuous Hamiltonian, the resulting integrator will be second-order accurate, symplectic, and (by construction) unit-length preserving (see Marsden and West [2001]). The symplectic form preserved by the numerical algorithm is not the weighted area form on $(\mathbb{S}^2)^N$ given in (3.1) but the two-form

$$\operatorname{Im}\left(\frac{\partial^2 L_d}{\partial(\varphi_k^{(0)})^\dagger \partial \varphi_k^{(1)}}\, d(\varphi_k^{(0)})^\dagger \wedge d\varphi_k^{(1)}\right),$$

where L_d is the discrete Lagrangian given in (5.2), which is an $\mathcal{O}(h)$ perturbation of it (see Rowley and Marsden [2002]).

6 Numerical results

Throughout this section, we will compare the behavior of the Hopf integrator with a number of other integrators:

1. A standard, non-variational integrator: we chose a standard explicit 4th-order Runge–Kutta method (RK4), composed with projection onto the unit sphere in order to preserve the unit-length constraint. It is well known (see e.g. Hairer, Lubich, and Wanner [2002]) that the resulting method is still 4th-order in time.

2. The implicit midpoint method on $\mathbb{S}^2$, given by

$$\frac{\mathbf{x}_k^{n+1} - \mathbf{x}_k^n}{h} = \frac{1}{4\pi} \sum_{j \neq k} \Gamma_j \frac{\mathbf{x}_j^{n+1/2} \times \mathbf{x}_k^{n+1/2}}{1 + \sigma^2 - \mathbf{x}_k^{n+1/2} \cdot \mathbf{x}_j^{n+1/2}}. \tag{6.1}$$

   This is just the standard midpoint method, applied to the vortex equations (1.6). Note that for this vector field, the implicit midpoint method in fact stays on the unit sphere without the need for an explicit projection. To see this, take the dot product of both sides of the equation with $\mathbf{x}_k^{n+1/2}$ and observe that the right-hand side vanishes, so that we get

$$(\mathbf{x}_k^{n+1} - \mathbf{x}_k^n) \cdot \mathbf{x}_k^{n+1/2} = 0,$$

which is equivalent to $\|\mathbf{x}_k^n\| = \left\|\mathbf{x}_k^{n+1}\right\|$, i.e., the length is preserved. This is not a general feature of the midpoint method, but is a consequence of the particular form of the point vortex equations. Furthermore, the midpoint method is symmetric under the interchange $\mathbf{x}_k^n \leftrightarrow \mathbf{x}_k^{n+1}$, $h \leftrightarrow -h$, and as a result the method seems to have excellent long-term conservation properties. To the best of our knowledge, it is not known if this version of the midpoint method on the sphere is symplectic.

3. The Lie group method of Engø and Faltinsen [2002], applied to the point vortex equations of Section 3. This second-order method preserves the vortex moment explicitly, and is a self-adjoint Lie group method, resulting in bounded energy error. However, this method is not symplectic (see Zhong and Marsden [1988]). This method is implemented by solving

$$y_1 = \mathrm{Ad}^*_{\exp(-\xi)}(y_0), \quad \text{with} \quad \xi = \frac{h}{2}\left(\nabla H(y_0) + \nabla H(y_1)\right),$$

where H is the point vortex Hamiltonian (3.2), y_0, y_1 are the point vortex locations in $\mathbb{R}^3$, viewed as the dual $\mathfrak{so}(3)^*$ of the Lie algebra of the rotation group, and $\mathrm{Ad}^*_g(y_0) = g y_0 g^{-1}$.

Our conclusion is that all three geometric methods outperform 4th-order Runge–Kutta with projection over moderately long time intervals. The Hopf and Lie–Poisson algorithms are roughly comparable in performance, while the midpoint method generally does better than either one: for one thing, the midpoint method conserves the vortex moment, a linear constant of the motion, exactly.

However, the conservation properties of the midpoint algorithm seem to be somewhat coincidental, and rely on the fact that for the point vortex equations, the algorithm stays on the unit sphere without reprojecting. It is therefore not clear how to generalize this algorithm to obtain, for instance, higher-order integrators with similar conservation properties. By contrast, for the variational Hopf integrator it suffices to start from a higher-order version of the discrete Lagrangian (5.1) to obtain a higher-order variational Hopf integrator.

6.1 Stable relative equilibria of vortex rings

Polvani and Dritschel [1993] have investigated the behavior of a ring of N equidistant vortices with the same strength Γ, placed on a circle of fixed longitude on the sphere (see Figure 6.1). They found that this configuration is a stable relative equilibrium, provided that $N \leq 7$ and that the longitude is higher than a certain critical value (dependent on N). For the case $N = 6$, the critical longitude is given by $z_c = 2/\sqrt{5}$ and the stable relative equilibria satisfy $z_0 > z_c$. The vortex ring rotates around the z-axis with angular velocity $\Omega = (N-1)\frac{\Gamma}{4\pi}\frac{z_0}{1-z_0^2}$.

For our simulation, we choose $N = 6$, $\Gamma = 1/6$ and $z_0 = 0.92$, so that $\Omega \approx 0.397$ and the period $T \approx 15.819$. The motion of the first vortex over a number of periods is illustrated in Figure 6.1.

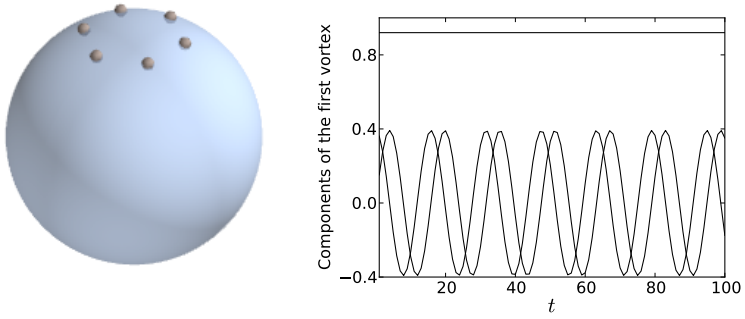

Figure 6.1: Left: Initial conditions for the 6-vortex Polvani-Dritschel vortex ring. Right: x, y and z-component of the first vortex in the Polvani-Dritschel simulation, where the time-step $h = 0.1$. The trajectory is clearly seen to be periodic.

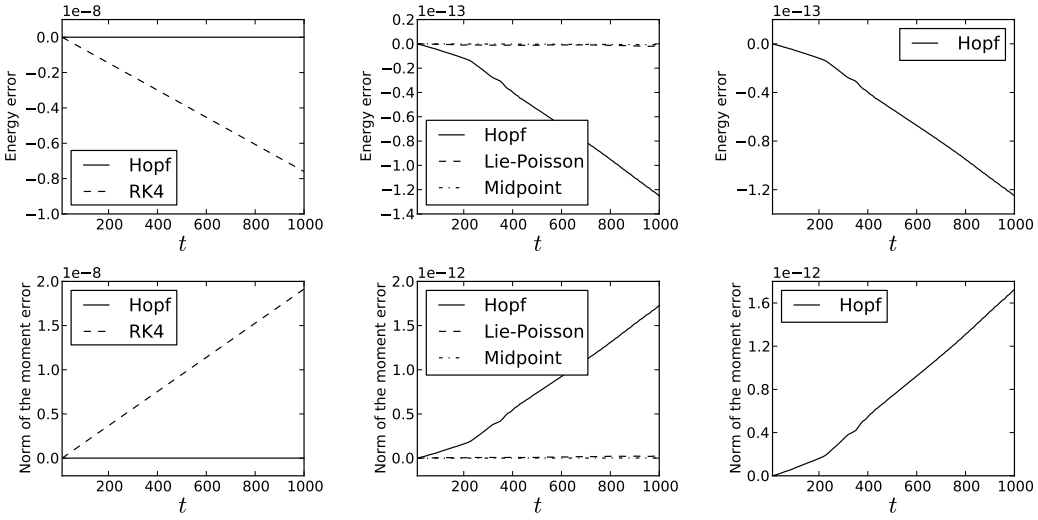

Figure 6.2: Comparison of the energy and momentum preservation between the geometric integrators, including our Hopf method, and 4th-order Runge–Kutta over moderate integration times. Runge–Kutta exhibits a small secular drift in the energy and momentum (left panes), while the energy and momentum are practically conserved for the geometric integrators (right panes). Here $h = 0.1$ and $\sigma = 0.0$. The small drift in the energy-momentum error for the Hopf integrator is due to round-off error.

Comparison with other integrators. We next turn to the energy and momentum conservation properties of the numerical integrator. We simulate the motion of the Polvani-Dritschel vortex ring with time step $h = 0.1$ and regularization parameter $\sigma = 0.0$, for $T = 1000$ units of time, using all four integrators.

In Figure 6.2 we have plotted the energy error $\Delta E := E(t_n) - E(t_0)$ (top row of figures) and the moment error $\Delta M := \|\mathbf{M}(t_n) - \mathbf{M}(t_0)\|$ (bottom row of figures) as a function of time. Runge–Kutta exhibits a small drift in the energy and momentum

error (left panes), whereas the energy and momentum are practically conserved for the geometric integrators (center panes). For the Hopf integrator, there is a much smaller drift in the energy and moment error, which is presumably due to the fact that one step of the Hopf integrator consists of a step with the forward method (5.28) followed by a step with the adjoint method (5.27). The error in these underlying one-step methods almost cancels out, up to some round-off error which is seen on the figure.

On the right panes of Figure 6.2, it can be seen that the Hopf integrator exhibits a small drift in the energy and moment, which is of the order $10^{-13} - 10^{-12}$ over 10^3 units of time. We conjecture that this is due to the way in which the Hopf integrator is implemented. Since a relative equilibrium is being tracked, we compute an essentially constant Lie group element $U^{(n)}$ at each update, and we multiply the previous vortex location $\varphi^{(n-1)}$ by this matrix to obtain the current location $\varphi^{(n)}$. As $U^{(n)}$ is essentially constant, round-off errors in the definition of φ accumulate rather than cancelling out on average, resulting in the slight linear trend observed in the figures. This roundoff error accumulation could be mitigated by the use of compensated summation techniques.

Numerical order calculation. We know from theoretical considerations that the Hopf integrator is second-order accurate, and so are the two other geometric methods. We now illustrate this statement by comparing the solution trajectories generated by the Hopf integrator with the exact trajectories. For 10 choices of time step h between 10^{-4} and 10^{-1} we run the simulation over $T = 100$ units of time and we compute the absolute error between the numerical and the exact solution. We consider only the first vortex, since the trajectories of the other vortices differ from the first by a rigid rotation. More precisely, for each integrator we do the following: if $\mathbf{x}_{\text{exact}}(t_n)$ is the exact position of the first vortex at time $t_n = nh$ and $\mathbf{x}_{\text{int}}^{n,h}$ is the numerical trajectory, then we compute

$$\Delta_h := \max_n \left\| \mathbf{x}_{\text{exact}}(t_n) - \mathbf{x}_{\text{int}}^{n,h} \right\|$$

for each of the selected time steps.

Figure 6.3 (left) shows a plot of absolute errors versus time steps for the three geometric integrators. All three integrators are of roughly second order. On the right pane of Figure 6.3, we have plotted the obtained accuracy for each of the three geometric methods as a function of the expended CPU time. We see that the Hopf and Lie–Poisson methods are roughly equivalent in terms of efficiency, with the midpoint method slightly more efficient, but we caution against reading too much into this figure, as the results depend heavily on the implementation of the method.

The μ-Hopf integrator. For our last simulation involving the Polvani-Dritschel vortex ring, we revisit the choice of the μ-component in propositions 5.2 and 5.3. We have so far chosen the solution corresponding to $\mu = 0$, as this solution was computationally easier to characterize. There is, however, no a priori reason to

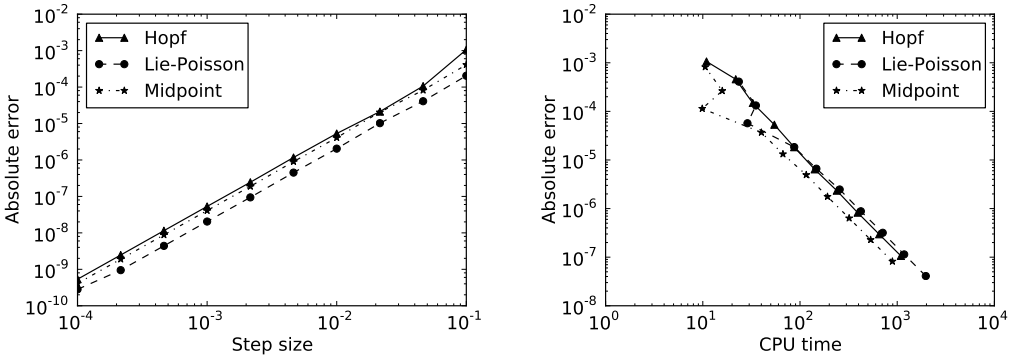

Figure 6.3: Left: Absolute error for each of the three integrators for the Polvani-Dritschel vortex ring over $T = 100$ units of time. All three integrators are second-order accurate in time. Right: Absolute error as a function of CPU time expended, again for $T = 100$ units of time. All three integrators show the same scaling in terms of attaining a certain accuracy for a fixed computational time.

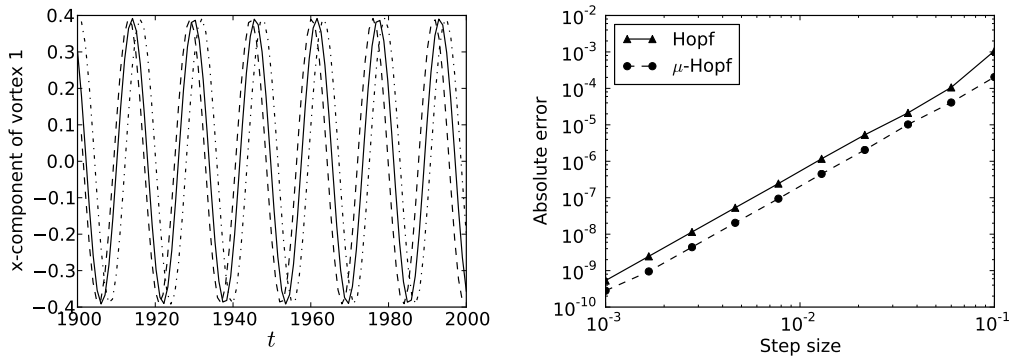

Figure 6.4: Comparison of the regular Hopf and the μ-Hopf algorithm. Left: Simulation of the x-component of the first vortex, step size $h = 0.5$. The solid line represents the exact trajectory, while the dashed and the dash-dotted line represent the Hopf and the μ-Hopf algorithm, respectively. Both numerical algorithms stay close to the exact trajectory over long integration times. Right: absolute error versus step size for the two Hopf algorithms. Both algorithms exhibit similar second-order accuracy in time.

prefer the $\mu = 0$ solution over the one for which $\mu \neq 0$. To corroborate this statement numerically, we have implemented the Hopf numerical algorithm choosing the solution corresponding to $\mu \neq 0$ for the direct equation (5.15) and the adjoint equation (5.25). The resulting numerical algorithm is *not* equivalent to the original Hopf algorithm, and has been termed the *μ-Hopf algorithm*.

In Figure 6.4, we compare both versions of the Hopf algorithm. For the simulation on the left, we simulated the motion of the Polvani-Dritschel ring over $T = 2000$ units of time with step size $h = 0.5$. The last 100 units of time of the simulation

are shown for both integrators, together with a plot of the exact solution. We see that both integrators, although not equivalent, track the exact solution well. On the right, we have plotted the absolute error versus the step size employed, and we see that both the regular Hopf as well as the μ-Hopf integrator are second-order accurate.

6.2 The spherical von Kármán vortex street

An important class of relative equilibria consists of the single and double von Kármán vortex streets on the sphere described by Chamoun, Kanso, and Newton [2009]. The single vortex street consists of two staggered arrays of vortices, each consisting of N equidistant vortices of strength Γ, at fixed colatitudes $\phi = \phi_1$ and $\phi = \pi - \phi_1$, together with vortices of strength Γ_n and Γ_s at the north and the south pole, respectively (see Figure 6.5).

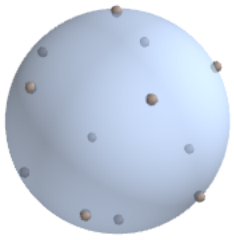

Figure 6.5: The spherical von Kármán vortex street consists of two staggered latitudinal layers of 5 vortices, together with vortices at the North and South pole of the sphere.

For the simulations in this section, we take the number of vortices in each ring to be $N = 5$, and we set the colatitude equal to $\phi_1 = \pi/3$. The vortex strength for the ring vortices is set equal to unity, $\Gamma = 1$, while the polar vortices satisfy $\Gamma_n = -\Gamma_s = 1/2$. This configuration forms a relative equilibrium which rotates around the z-axis with period $T = 10.85$. Based on the behavior of the planar Von Kármán vortex street, it is believed that this relative equilibrium is unstable, although no rigorous stability analysis exists, to the best of our knowledge.

Short integration times. In Figure 6.6 we compare the energy behavior of the Hopf variational integrator with that of the 4th-order Runge–Kutta method, for short amounts of time. Both simulations use a step size $h = 0.1$ and no regularization, i.e. $\sigma = 0$. Over the first 100 units of time, the vortices move as a relative equilibrium, and we see that the variational integrator preserves the energy almost exactly, in contrast to Runge–Kutta. When the simulation time is close to $t = 100$, a small uptick in the energy and moment error can be seen. This deviation from energy/moment preservation signals the onset of instability of the relative equilibrium, as will become clear from longer simulations.

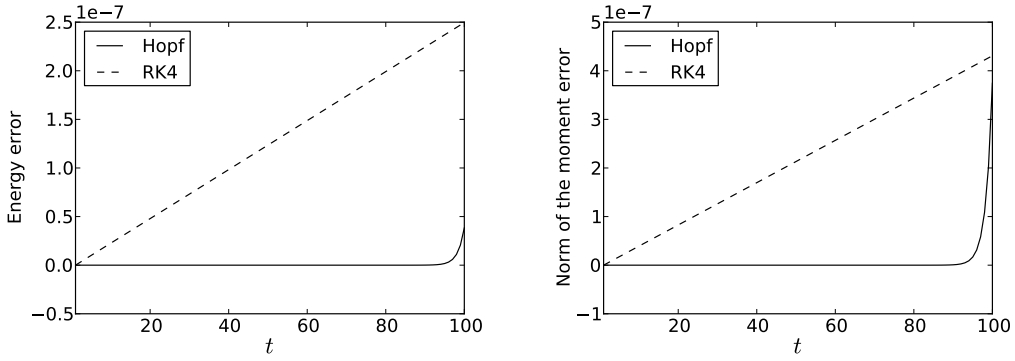

Figure 6.6: For a relative equilibrium, the variational integrator (line) preserves the energy (left) and moment (right) almost exactly, compared to 4th-order Runge–Kutta (dashed), until the onset of instability close to $t = 100$.

Longer integration times. For longer integration times, the equilibrium becomes unstable and breaks up, leading to aperiodic motion of the vortices. In this regime, the energy is no longer exactly preserved by the Hopf integrator, but exhibits bounded oscillations, as is to be expected from a symplectic integrator. In Figure 6.7 we have plotted both the energy error as well the error in the norm of the vortex moment for each of the integrators. The simulation uses time step $h = 0.3$ and regularization parameter $\sigma = 0.25$ and runs over 1000 time units.

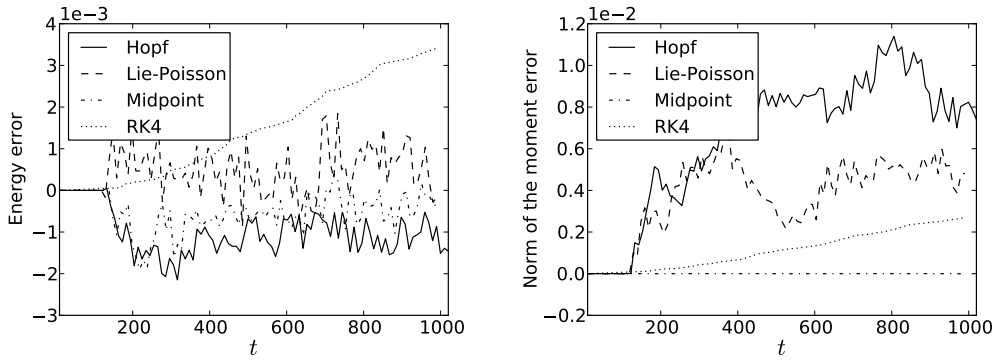

Figure 6.7: Comparison of the energy (left) and momentum conservation (right) between the geometric integrators and 4th-order Runge–Kutta. The step size is $h = 0.3$ and the regularization parameter is $\sigma = 0.25$. Hopf integrator: dark blue, solid line; Lie–Poisson integrator: green, dashed line; projected midpoint integrator: red, dash-dot line; RK4: light blue, dotted line.

The geometric integrators clearly exhibit bounded oscillations in the energy and the norm of the moment, whereas these quantities grow linearly in time for 4th-order Runge–Kutta.

6.3 Collapse of three vortices

It is well known that certain configurations of point vortices on the sphere will collapse to a point in finite time. For 3 vortices, necessary and sufficient conditions for collapse were given by Kidambi and Newton [1998] while Sakajo [2008] identified an open set of initial conditions for collapse of 4 vortices. We focus here on the case of 3 vortices.

We simulate the motion of three vortices with strengths $\Gamma_1 = \Gamma_2 = 1$, $\Gamma_3 = -1/2$ placed at the vertices of a triangle with side lengths $l_{12} = \sqrt{3}/2$, $l_{23} = \sqrt{2}/2$ and $l_{31} = 1$. For this configuration, it can be calculated that collapse occurs after $\tau_- \equiv 4\pi(\sqrt{23} - \sqrt{17}) \cong 8.4537$ units of time. The trajectories of the colliding vortices are shown in Figure 6.8. Note that these initial conditions are for the unregularized system, i.e. (1.6) with $\sigma = 0$. Adding some regularization to the system effectively amounts to imposing a minimum distance on the vortices and will prevent the vortex configuration from collapsing to a single point.

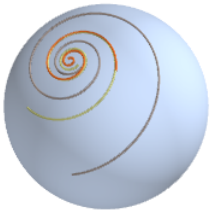

Figure 6.8: Trajectories of 3 colliding vortices, for the initial conditions described in the text.

We simulate the system first with a moderate time step, $h = 0.1$, and some amount of regularization, $\sigma = 0.10$, for $T = 15$ units of time. On Figure 6.9 we see that the geometric integrators, including the Hopf integrator, perform a better job of preserving the energy and vortex moment than Runge–Kutta: while all integrators show some buildup in the energy and moment error around the time of the collapse, the energy and moment return to their original values after the collapse for the geometric integrators, but settle down at a different value for Runge–Kutta.

For long-term simulations, this effect is even more pronounced. After the near-collapse, the three vortices travel past each other and (nearly) collapse again at a later time, a situation which repeats itself periodically afterwards. Figure 6.10 shows that for every collapse event, the Runge–Kutta simulation incurs a jump in the energy and the moment, whereas the geometric integrators manage to preserve these invariants without any noticeable secular trend. Note also that the period of time between two collapse events increases gradually for Runge–Kutta, but stays (roughly) constant for the geometric integrators.

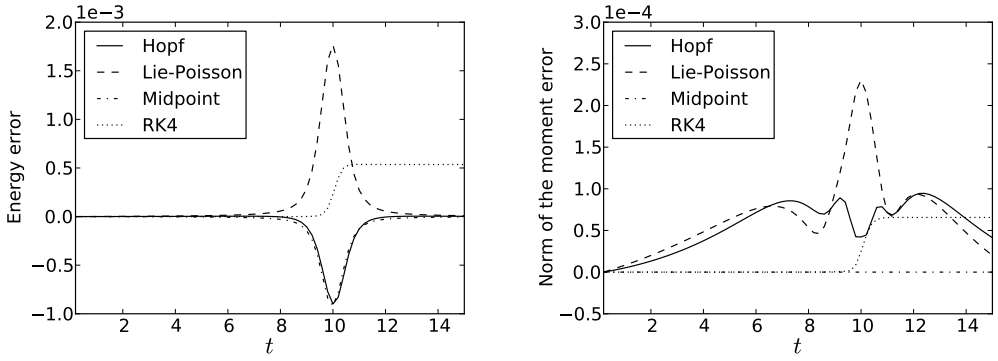

Figure 6.9: Energy (left) and moment (right) conservation for the geometric integrators and 4th-order Runge–Kutta close to vortex collapse, which happens for the unregularized system at $t \approx 8.45$. While RK4 conserves the energy and moment better than the geometric integrator up to the collapse, the energy and moment settle down in a different value after collapse. Here, $h = 0.1$ and $\sigma = 0.1$.

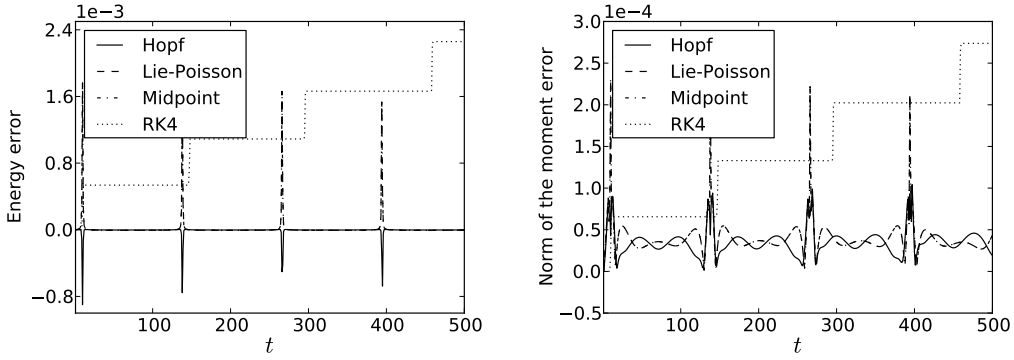

Figure 6.10: Numerical simulation of colliding point vortices for $T = 500$ units of time, where $h = 0.1$ and $\sigma = 0.10$. At regular instances of time, there are collapse events, but whereas the energy for the geometric integrators quickly returns to its original value after a collapse event, the energy and moment for Runge–Kutta increases in jumps at each collapse.

6.4 Large ensembles of vortices

We simulate the motion of 40 vortices of strength $\Gamma = 1/8$, distributed randomly over the surface of the sphere. The regularization parameter is set to $\sigma = 0.1$ and the step size is $h = 0.01$. For short integration times ($T = 20$), as can be seen from Figure 6.11, both the Hopf and the Lie–Poisson integrator exhibit bounded energy error, and they preserve the unit length constraint almost up to machine precision.

For moderate integration times ($T = 200$, with again $h = 0.01$ and $\sigma = 0.1$), we have that the energy is almost preserved by all three integrators, up to a small, bounded error; see Figure 6.12. For the vortex moment, we have that the midpoint integrator

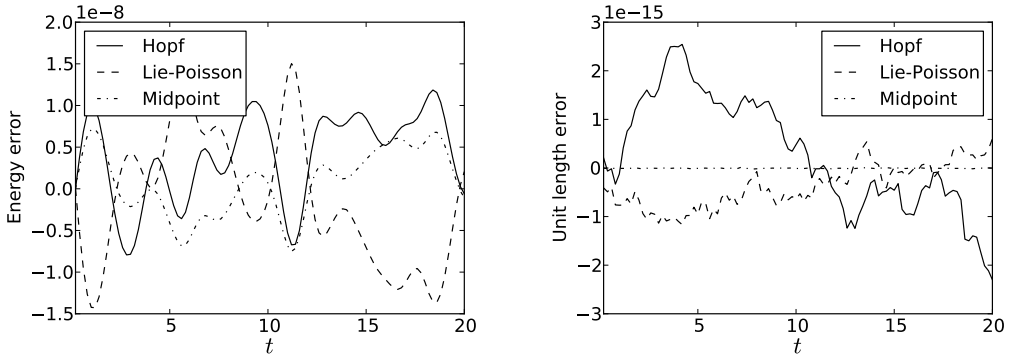

Figure 6.11: Left: Energy error for the motion of 40 random point vortices. Right: Preservation of the unit length constraint.

seems to preserve this invariant exactly, while both the Hopf and the Lie–Poisson integrator exhibit a small error consistent with the order of the discretization. In this figure, the midpoint method is not included, as it preserves the vortex moment exactly.

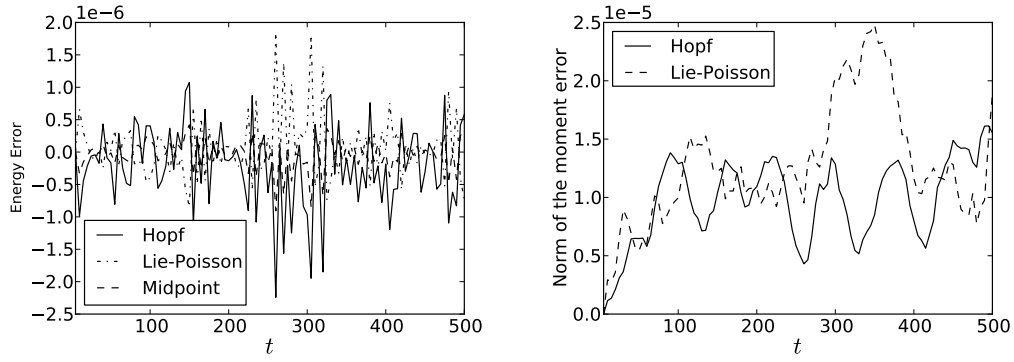

Figure 6.12: Energy error (left) and moment error (right) for the motion of 40 random point vortices over 200 units of time. The geometric integrators exhibit similar conservation properties for the energy and the moment.

7 Conclusions and outlook

In this paper, we have used the Hopf fibration to construct a linear Lagrangian on the three-sphere $\mathbb{S}^3$, whose Euler–Lagrange equations project down to the point vortex equations on $\mathbb{S}^2$. We have used this Lagrangian formulation to construct a variational integrator for point vortices on the sphere, and we have used the isomorphism between $\mathbb{S}^3$ and $SU(2)$ to ensure that the unit-length constraint in $\mathbb{S}^3$

is automatically satisfied. Below, we discuss some possibilities for future research.

Extension to higher-order integrators. Our Lagrangian approach to the construction of discrete point vortex integrators can be extended without major difficulties to the construction of integrators whose numerical order is higher than two. It suffices to take a discretization in (5.1) which is of higher than second order. The standard theory of Lagrangian variational integrators (see Marsden and West [2001]) then ensures that the resulting discrete equations of motion will have the same order of accuracy as the discrete Lagrangian.

Other Lie group methods. We have constructed a Lie group variational integrator by discretizing the linear Lagrangian (4.5) and writing the update map in terms of $SU(2)$-matrices. Another approach is due to Bou-Rabee and Marsden [2009] (see also Kobilarov and Marsden [2011]). Here the Lagrangian is first written in a left-trivialization of $TSU(2) \cong SU(2) \times \mathfrak{su}(2)$ by mapping $(g, \dot{g})$ to (g, ξ), where $g^{-1}\dot{g} = \xi$, and this equation is then discretized and added to the variational principle using a Lagrange multiplier, giving rise to the so-called *Hamilton-Pontryagin variational principle*. A similar variational principle, known as the *Clebsch variational principle*, was pioneered in Cotter and Holm [2009]. It would be of considerable interest to discretize our linear Lagrangian (4.5) using these augmented variational principles and to compare the properties of the resulting discrete mechanical system with our straightforward discretization.

Statistical mechanics of large numbers of point vortices. The statistical theory of vortex motion set forth in Onsager [1949] predicts that, under certain energetic conditions, like-signed vortices will tend to cluster over time. We have not attempted to extract any statistical information from the simulation of large number of vortices on the sphere, but it would be of considerable interest to do so. To alleviate the $O(N^2)$-cost of computing the point vortex Hamiltonian while maintaining the symplectic nature of the integrator, a geometric fast multipole method like the one developed in Chartier, Darrigrand, and Faou [2010] could be used.

Vorticity distributions on the sphere and other surfaces. Point vortices represent the simplest non-trivial distributions of vortices on the sphere. The methods proposed in this paper are expect to generalize without any significant difficulty to the case of vortex blobs or patches of vorticity on the sphere (see Chorin [1973]; Newton [2001]).

To treat vortical distributions on other surfaces, the following construction from prequantization could be used. Recall that the Hopf fibration is the fiber bundle associated to the quantum line bundle on $\mathbb{S}^2$ associated with the area form; see e.g. Woodhouse [1992]. For the motion of point vortices on a surface Σ with integral area form, one can follow a similar route and lift the motion of the vortices to (the

principal fiber bundle associated to) the quantum line bundle, for which a similar relation as (2.14) will continue to hold.

Moreover, PDEs such as the KdV and nonlinear Schrödinger equation can also be formulated using a linear Lagrangian, and we hope that the methods introduced in this paper may be useful for these systems as well.

Acknowledgments

We would like to dedicate this paper to the memory of Hassan Aref, whose kind encouragement and insightful remarks at the 2010 SIAM-SEAS meeting provided the initial stimulus for this work. Furthermore, we would like to thank J. D. Brown, C. Burnett, F. Gay-Balmaz, M. Gotay, D. Holm, E. Kanso, S. D. Kelly, P. Newton, T. Ohsawa, B. Shashikanth and A. Stern for stimulating discussions and helpful remarks.

M. L. and J. V. are partially supported by NSF grants DMS-1010687 and DMS-1065972. J. V. is on leave from a Postdoctoral Fellowship of the Research Foundation–Flanders (FWO-Vlaanderen). This work is supported by the IRSES project GEOMECH (nr. 246981) within the 7th European Community Framework Programme.

A Analysis of a planar vortex integrator

In this appendix, we show that the integrator of Rowley and Marsden [2002] for point vortices in the plane shares a number of remarkable features with the Hopf integrator, which stem from the fact that both systems are derivable from a linear Lagrangian. Similar observations, but for the numerical integration of canonical Hamiltonian systems, were made by Brown [2006].

Decomposition into one-step methods. Rowley and Marsden [2002] start from the linear Lagrangian (1.3), which they discretize by setting

$$L_d(z_0, z_1) = hL\left((1-\alpha)z_0 + \alpha z_1, \frac{z_1 - z_0}{h}\right),$$

where $\alpha \in [0,1]$ is a real interpolation parameter. The equations of motion derived from this Lagrangian are given by

$$\frac{z_{n+2} - z_n}{2h} = \alpha f(z_{n+\alpha}) + (1-\alpha) f(z_{n+1-\alpha}), \tag{A.1}$$

where $z_{n+\alpha} := (1-\alpha)z_n + \alpha z_{n+1}$ and $f(z)$ is the right-hand side of the vortex equations (1.1). It turns out that for $\alpha = 1/2$, they can be written as the composition of a one-step method and its adjoint. To see this, we specialize to the case $\alpha = 1/2$ and use the fact that the original Lagrangian L is linear in the velocities to write

$$L_d(z_0, z_1) = L(z_{1/2}, z_1) - L(z_{1/2}, z_0),$$

and we define $L_{d,+}(z_0, z_1, h) := L(z_{1/2}, z_1)$ and $L_{d,-}(z_0, z_1, h) := -L(z_{1/2}, z_0)$, so that $L_d = L_{d,+} + L_{d,-}$. Consider the *adjoint* L_d^* of a discrete Lagrangian L_d, which is defined by $L_d^*(z_0, z_1, h) := -L_d(z_1, z_0, -h)$ (see Marsden and West [2001]). Then, we have that

$$L_{d,+}^*(z_0, z_1, h) = L_{d,-}(z_0, z_1, h),$$

and vice versa. This definition is motivated by the fact that the adjoint of the discrete Euler–Lagrange flow of a discrete Lagrangian is given by the discrete Euler–Lagrange flow of the adjoint discrete Lagrangian.

The composition of the discrete Euler–Lagrange flow of two discrete Lagrangians is given by the discrete Euler–Lagrange flow of a composition discrete Lagrangian that is the sum of the two original discrete Lagrangians. As a result, the discrete Euler–Lagrange flow for L_d is given by the composition of the discrete Euler–Lagrange flows for $L_{d,+}$ and its adjoint $L_{d,+}^* = L_{d,-}$. These discrete flows can be viewed as one-step methods, and are typically only first-order accurate, but their composition is symmetric and therefore has even order of accuracy, and is, in particular, second-order accurate.

Lastly, we remark that for the point-vortex Lagrangian (1.3) the discrete Lagrangians $L_{d,+}$ and $L_{d,-}$ *coincide*, which means that each of them are self-adjoint. As a result, the underlying one-step method is second-order. In fact, it can easily be seen that for $\alpha = 1/2$, the point vortex equations (A.1) can be written as the composition of the implicit midpoint method

$$\frac{z_{n+1} - z_n}{h} = f(z_{n+1/2})$$

with itself. This method is clearly second-order accurate.

For the case of point vortices on the sphere the Lagrangians $L_{d,+}$ and $L_{d,-}$ still coincide, but in order to recover the equations of motion (5.4) and to enforce the constraint $\langle \varphi^{n+1}, \varphi^{n+1} \rangle = 1$, different constraint forces have to added to the discrete flow. As a result, the underlying one-step methods (5.10) and (5.11) no longer coincide and are individually only first-order accurate, although their composition is second-order accurate.

The choice $\alpha = 0, 1$ for the interpolation parameter. The method (A.1) is implicit for all choices of α except $\alpha = 0, 1$, in which case the equations become

$$\frac{z_{n+2} - z_n}{2h} = f(z_{n+1}).$$

This method turns out to be the *symmetric explicit midpoint method* (see Hairer, Lubich, and Wanner [2002]), which is well-known to exhibit parasitic oscillatory solutions. These solutions can easily be observed in the dynamics of point vortices: in Figure A.1, we have plotted the energy error for a simulation of a four-vortex problem with vortex strengths $\Gamma = (.1, .3, -.2, -.4)$ and initial conditions $z = (0, .5i, 1, .7 + .6i)$. For the simulation where $\alpha = 0.9$ the energy error is bounded,

while for the simulation employing $\alpha = 1.0$ there is a clear linear drift in the energy error. The time step used for both simulations was $h = 0.1$.

This is in clear contrast to the construction of variational integrators for *nondegenerate* Lagrangians, for which any choice of interpolation parameter α will result in a stable, second-order integrator.

Similar instabilities exist for the case of point vortices on the sphere: the discrete equations (5.6), for instance, exhibit a clear secular drift in the energy, despite being variational.

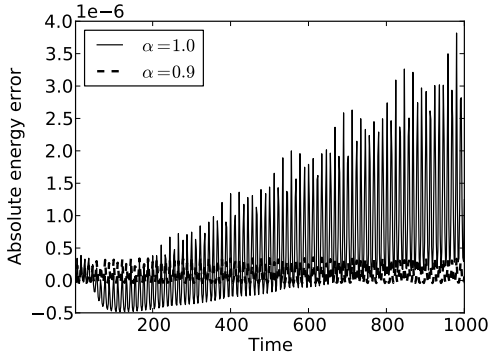

Figure A.1: For the four-vortex problem described in the text, the energy error exhibits a linear drift for the integrator with $\alpha = 1$ (solid line) but stays bounded whenever $\alpha \neq 1$; here $\alpha = 0.9$ is shown (dashed line).

References

Aref, H. [2007], Point vortex dynamics: a classical mathematics playground, *J. Math. Phys.* **48**, 065401, 23.

Aref, H. [2011], Relative equilibria of point vortices and the fundamental theorem of algebra, *Proceedings of the Royal Society A: Mathematical, Physical and Engineering Science* **467**, 2168–2184.

Birkhoff, G. D. [1966], *Dynamical systems.* With an addendum by Jurgen Moser. American Mathematical Society Colloquium Publications, Vol. IX. American Mathematical Society, Providence, R.I.

Bogomolov, V. A. [1977], Dynamics of vorticity at a sphere, *Fluid Dynamics* **12**, 863–870. 10.1007/BF01090320.

Borisov, A. V., I. S. Mamaev, and A. A. Kilin [2004], Absolute and relative choreographies in the problem of point vortices moving on a plane, *Regul. Chaotic Dyn.* **9**, 101–111.

Bou-Rabee, N. and J. E. Marsden [2009], Hamilton-Pontryagin integrators on Lie groups. I. Introduction and structure-preserving properties, *Found. Comput. Math.* **9**, 197–219.

Boyland, P., M. Stremler, and H. Aref [2003], Topological fluid mechanics of point vortex motions, *Physica D: Nonlinear Phenomena* **175**, 69 – 95.

Brown, J. D. [2006], Midpoint rule as a variational-symplectic integrator: Hamiltonian systems, *Phys. Rev. D* **73**, 024001.

Bruveris, M., D. C. P. Ellis, D. D. Holm, and F. Gay-Balmaz [2011], Un-reduction, *J. Geom. Mech.* **3**, 363–387.

Cendra, H. and J. E. Marsden [1987], Lin constraints, Clebsch potentials and variational principles, *Phys. D* **27**, 63–89.

Chamoun, G., E. Kanso, and P. K. Newton [2009], Von Kármán vortex streets on the sphere, *Physics of Fluids* **21**, 116603.

Chapman, D. M. F. [1978], Ideal vortex motion in two dimensions: Symmetries and conservation laws, *Journal of Mathematical Physics* **19**, 1988–1992.

Chartier, P., E. Darrigrand, and E. Faou [2010], A regular fast multipole method for geometric numerical integrations of Hamiltonian systems, *BIT* **50**, 23–40.

Chorin, A. J. [1973], Numerical study of slightly viscous flow, *J. Fluid Mech.* **57**, 785–796.

Cotter, C. J. and D. D. Holm [2009], Continuous and discrete Clebsch variational principles, *Found. Comput. Math.* **9**, 221–242.

Engø, K. and S. Faltinsen [2002], Numerical Integration of Lie-Poisson Systems while Preserving Coadjoint Orbits and Energy, *SIAM Journal on Numerical Analysis* **39**, pp. 128–145.

Faddeev, L. and R. Jackiw [1988], Hamiltonian reduction of unconstrained and constrained systems, *Phys. Rev. Lett.* **60**, 1692–1694.

Frankel, T. [2004], *The Geometry of Physics: An Introduction*. Cambridge University Press, Cambridge, second edition.

Hairer, E., C. Lubich, and G. Wanner [2002], *Geometric numerical integration*, volume 31 of *Springer Series in Computational Mathematics*. Springer-Verlag, Berlin, 1st edition.

Kidambi, R. and P. K. Newton [1998], Motion of three point vortices on a sphere, *Phys. D* **116**, 143–175.

Kimura, Y. and H. Okamoto [1987], Vortex Motion on a Sphere, *J. Phys. Soc. Japan* **56**, 4203–4206.

Kobilarov, M. and J. Marsden [2011], Discrete Geometric Optimal Control on Lie Groups, *IEEE Transactions on Robotics* **27**, 641 –655.

Kostant, B. [2005], Minimal coadjoint orbits and symplectic induction. In *The breadth of symplectic and Poisson geometry*, volume 232 of *Progr. Math.*, pages 391–422. Birkhäuser Boston, Boston, MA.

Lamb, H. [1945], *Hydrodynamics*. Dover Publications. Reprint of the 1932 Cambridge University Press edition.

Lee, T., M. Leok, and N. H. McClamroch [2007], Lie group variational integrators for the full body problem, *Comput. Methods Appl. Mech. Engrg.* **196**, 2907–2924.

Lemaître, G. [1948], Quaternions et espace elliptique, *Pont. Acad. Sci. Acta* **12**, 57–78.

Leok, M. and J. Zhang [2011], Discrete Hamiltonian variational integrators, *IMA Journal of Numerical Analysis* **31**, 1497–1532.

Lim, C., J. Montaldi, and M. Roberts [2001], Relative equilibria of point vortices on the sphere, *Phys. D* **148**, 97–135.

Ma, Z. and C. W. Rowley [2010], Lie-Poisson integrators: a Hamiltonian, variational approach, *Internat. J. Numer. Methods Engrg.* **82**, 1609–1644.

Majda, A. J. and A. L. Bertozzi [2002], *Vorticity and incompressible flow*, volume 27 of *Cambridge Texts in Applied Mathematics*. Cambridge University Press, Cambridge.

Marsden, J. E. and M. West [2001], Discrete mechanics and variational integrators, *Acta Numerica* **10**, 357–514.

Milne-Thomson, L. [1968], *Theoretical hydrodynamics.* London: MacMillan and Co. Ltd., fifth edition, revised and enlarged edition.

Montgomery, R. [2002], *A tour of subriemannian geometries, their geodesics and applications*, volume 91 of *Mathematical Surveys and Monographs*. American Mathematical Society, Providence, RI.

Moser, J. and A. Veselov [1991], Discrete versions of some classical integrable systems and factorization of matrix polynomials, *Comm. Math. Phys.* **139**, 217–243.

Newton, P. K. [2001], *The N-vortex problem. Analytical techniques*, volume 145 of *Applied Mathematical Sciences*. Springer-Verlag, New York.

Newton, P. K. and T. Sakajo [2011], Point vortex equilibria and optimal packings of circles on a sphere, *Proceedings of the Royal Society A: Mathematical, Physical and Engineering Science* **467**, 1468–1490.

Novikov, S. P. [1982], The Hamiltonian formalism and a many-valued analogue of Morse theory, *Russian Mathematical Surveys* **37**, 1.

Oh, Y.-G. [1997], Symplectic topology as the geometry of action functional. I. Relative Floer theory on the cotangent bundle, *J. Differential Geom.* **46**, 499–577.

Onsager, L. [1949], Statistical hydrodynamics, *Nuovo Cimento (9)* **6**, 279–287.

Pekarsky, S. and J. E. Marsden [1998], Point vortices on a sphere: stability of relative equilibria, *J. Math. Phys.* **39**, 5894–5907.

Polvani, L. M. and D. G. Dritschel [1993], Wave and vortex dynamics on the surface of a sphere, *J. Fluid Mech.* **255**, 35–64.

Rowley, C. and J. Marsden [2002], Variational integrators for degenerate Lagrangians, with application to point vortices. In *Proceedings of the 41st IEEE Conference on Decision and Control*, volume 2, pages 1521 – 1527.

Saffman, P. G. [1992], *Vortex dynamics*. Cambridge Monographs on Mechanics and Applied Mathematics. Cambridge University Press, New York.

Sakajo, T. [2008], Non-self-similar, partial, and robust collapse of four point vortices on a sphere, *Phys. Rev. E* **78**, 016312.

Soulière, A. and T. Tokieda [2002], Periodic motions of vortices on surfaces with symmetry, *Journal of Fluid Mechanics* **460**, 83–92.

Urbantke, H. K. [2003], The Hopf fibration — seven times in physics, *J. Geom. Phys.* **46**, 125–150.

von Helmholtz, H. [1858], Über Integrale der hydro-dynamischen Gleichungen, welche den Wirbelbewegungen entsprechen, *Journal für die reine und angewandte Mathematik (Crelles Journal)* **55**, 25–55.

Woodhouse, N. M. J. [1992], *Geometric quantization*. Oxford Mathematical Monographs. The Clarendon Press Oxford University Press, New York, second edition. Oxford Science Publications.

Zhong, G. and J. E. Marsden [1988], Lie-Poisson Hamilton-Jacobi theory and Lie-Poisson integrators, *Phys. Lett. A* **133**, 134–139.